Research article

Alginate functionalized sugarcane cellulose-based beads to improve methylene blue adsorption from aqueous solution

Huynh Vu Thanh Luong [a,b,*], Phuoc Pha Le [a], Quang Quoc Viet Thieu [b], Viet Nhan Hoa Nguyen [b], Thi Nhu Y. Nguyen [c]

[a] Applied Chemical Engineering Lab, Can Tho University, Can Tho, 94000, Viet Nam
[b] Faculty of Chemical Engineering, Can Tho University, Can Tho, 94000, Viet Nam
[c] Can Tho University of Technology, Can Tho, 94000, Viet Nam

A R T I C L E   I N F O

A B S T R A C T

The study was carried out with the goal of synthesizing composite bead of cellulose, chitosan functionalized by sodium alginate using as an efficient and applicable adsorbent for methylene blue removal. Fabricating parameters of the material synthesis process like cellulose mass, sodium hydroxide concentration, immersing time and sodium alginate concentration were assessed in detail. The dye adsorption performance in water under the influence of pH, contact time, dye initial concentration, the material mass, shaking speed, temperature was also thoroughly evaluated. The results of advanced analyses showed that the beads were successfully synthesized with a rough surface and mesoporous structure. The adsorption isotherm and adsorption kinetics of dye adsorption process exhibited that the process was consistent with the Freundlich adsorption isotherm and the pseudo-second-order kinetic model, indicating a favorable physical adsorption process with multilayer of the dye on the adsorbent surface. The intra-particle diffusion model showed the strong dye adsorption by the beads occurred during the first two and half hours. The adsorbent could maintain its adsorption performance of 86 % for three times of regeneration. Finally, this study provided a recyclable and effective adsorbent for dyes separation from water.

1. Introduction

The problem of water pollution in the world has become more and more serious and is the subject of much attention, especially the textile industry. The amount of wastewater in the textile dyeing and bleaching stages in most textile factories contains a lot of toxic substances such as metals, dyes, high alkalinity, and high color [1,2]. Dyes often have stable structures that are difficult to biodegrade and are highly toxic to humans and animals [3]. One of the popular dyes in the textile industry is methylene blue (MB) – a cationic dye, which greatly causes the problems in water resources and on human health like eye burns, vomiting, diarrhea, methemoglobinemia, mutagenic, carcinogenic, and allergenic problems [2,4]. To remove dye from aqueous solution, physical and chemical treatments, e.g., coagulation-flocculation, and oxidation-reduction, have systematically investigated [5,6].

These techniques, nevertheless, have integral restrictions such as high cost, high energy consumption, and generation of hazardous by-products [7–9]. In dye treatments, adsorption is unique because it is a simple, effective technique that does not generate any potentially hazardous substances [10,11]. To fit a zero-waste tendency, plenty of publications about applying carbonaceous waste

---

* Corresponding author. Faculty of Chemical Engineering, Can Tho University, Can Tho, 94000, Viet Nam.
  E-mail address: lhvthanh@ctu.edu.vn (H.V.T. Luong).

were reported, especially from the agricultural by-products to prepare biosorbents [12–14]. The biosorbents are superior in many aspects, but difficulties encountered during separating spent these biosorbents and poor regeneration limit its potential usage in the treatment system. Therefore, it is necessary to generate a biosorbent derived from agricultural sector which is easily separated and reused after treatment process.

One of the early reports of using magnetic cellulose beads combining magnetic particles with cellulose and activated carbon for removing MB in aqueous solution showed that adsorption capacity is 2.13×10^{-3} mmol g^{-1} and these beads can be reused for 3 times [15]. However, the preparation process is so complicated and required a special equipment (submerged circulative impinging stream reactor). A similar study was conducted by Mokhtar et al. [16] using magadiite-chitosan composite beads to adsorb MB with adsorption capacity of 45.25 mg g^{-1}. These beads, however, possessed only positive charge surface in pH range of 4.0–12.0, causing a repulsive force when these beads are applied for adsorbing positive dyes likes MB. In 2021, Mokhtari et al. reported that chitosan/alginate/cellulose nanofibers successfully removed Eriochrome Black-T from aqueous solution [17]. Besides cellulose, chitosan and alginate in form of hydrogels [18] or beads [19] showed their ability to remove azo dyes from aqueous solution. Therefore, it is able to use a composite bead consisting of cellulose, chitosan and alginate to remove dyes from aqueous solution.

This work, for the first time, formulated alginate functionalized sugarcane cellulose-based beads (CC-SA) for effective adsorption of methylene blue in aqueous solution. In this study, the systems were conveniently synthesized with simple processes, cheap and widely available materials, sugarcane bagasse and chitosan, as a potential adsorbent for alginate modification. The main objective aimed to develop an economical adsorption material which is simply separable and recycled at ambient conditions. Methylene blue adsorption into CC-SA was investigated in terms of the adsorption capacity, Langmuir/Freundlich/Dubinin-Radushkevich isotherms, first/second-order kinetics and intraparticle diffusion process. Lastly, CC-SA recycling was investigated.

2. Materials and methods

2.1. Materials

Xilong Scientific (China) supplied calcium chloride (96 %), sodium hydroxide (96 %), sodium hypochlorite (8 %), potassium chloride (99.5 %), sulfuric acid (95–98 %), chlorohydric acid (36–38 %) ethanol (98 %) and hexane (99 %). Sodium alginate (95 %) was bought from Shanghai Zhanyun Chemical (China). All other chemicals were of analytical grades.

2.2. Recovery of cellulose from sugarcane baggage

The cellulose synthesis process is demonstrated in Fig. S1. Firstly, sugarcane baggage was collected from local market, then washed with warm distilled water and dried at 100 °C (SF 55, Memmert) for 24 h before mincing, grounding, and sieving using a 350 μm sieve (AS200 Control, Retsch). The cellulose was consequently recovered as the process in report of Hokkanen [20]. For this, 25 g of sugarcane baggage grounds were placed in 500-mL beaker containing 250 mL water and stirred at 80 °C for 1 h to remove sugar in the sugarcane baggage. This step was triplicated to remove the left sugar in the sugarcane baggage. The sample was then hydrolyzed with H_2SO_4 4 % (vol/vol) at 80 °C for 90 min, after that the sample was washed with distilled water by sonication (BUS3, OVAN). Lignin in the sample was subsequently removed by soaking in 80 °C NaOH solution 10 % (wt./vol) for 3 h and then the sample was washed using distilled water until neutral. The sample was then decolorized by using NaClO 2 % (wt./vol) at 50 °C for 3 h and lipid in the sample was removed by a 50/50 Hexane/Ethanol cosolvent (vol/vol) for 4 h via a Soxhlet system. Finally, cellulose was collected after washed and dried at 60 °C (SF 55, Memmert) for 24 h.

2.3. Recovery of chitosan from shrimp shells

The shrimp shells were collected from the local market at Can Tho city, Vietnam and directly pretreated to remove the impurities. The process consists of two periods, i.e., the 1st period is extraction of chitin from shrimp shell by using electrolysis method, the 2nd period is deacetylation of chitin using chemistry hydrolysis. To this end, the 1st period included three steps: the 1st step was to reduce protein from shrimp shell in cathode chamber containing sodium sulfate solution with the weight/volume ratio of shrimp shells/ $Na_2SO_4 = 1/40$ at electrical potential of 15 V for 90 min since pH in this chamber is 13.0 causing dissolution of amino acids in the shrimp shells. The 2nd step was to reduce minerals from the shrimp shells in anode chamber containing sodium sulfate solution with the identical condition as cathode chamber; however, the pH solution in anode chamber was 2.0 leading to dissolve $CaCO_3$ from the shrimp shells. The shrimp shells after the 2nd step were washed for 3 times using distilled water, then reduced protein again in the cathode chamber with the same condition, instead of increasing reaction time to 120 min, this was the 3rd step of the 1st period. The 2nd period was completed by deacetylation of 1 g chitin in 40 mL NaOH 40–50 % for 90–150 min at 110 °C in the reflux system. The solid after that were rinsed with distilled thrice and then dried at 60 °C (SF 55, Memmert) for 24 h to obtain the chitosan.

2.4. Synthesis of cellulose chitosan alginate (CC-SA) beads

According to the study of Nan & Renbi [21], CC-SA beads were synthesized by structurally functionalized cellulose/chitosan (CC) beads with alginate in a calcium chloride solution at ambient temperature. To this end, 0.1–0.5 g of cellulose was added to 50 mL distilled water and sonicated for 3 min. After that, chitosan 3 % (wt./vol) solution was added to the mixture and agitated for 30 min to obtain a homogenous mixture. Subsequently, CC beads were obtained by dropping the as-synthesized homogenous mixture into NaOH

0.25–1.25 M solution for 2 h before washing with distilled water until pH of filtrate got neutral. Finally, the CC beads were placed into sodium alginate solution of 0–4% (wt./wt.) and the mixture was agitated for 0–24 h. The formed cellulose/chitosan/alginate (CC-SA) beads were filtrated from the mixture using a Whatman membrane, rinsed with water thrice, and dried at 50 °C for 24 h.

2.5. Adsorption of methylene blue

To examine the ability of CC-SA beads in adsorbing methylene blue (MB) in aqueous solution, effective parameters like pH, contact time, initial concertation of MB, adsorbent mass, speed of agitation, and temperature were investigated. For this, 100 mL of MB at a concentration of 5–25 mg L^{-1} with pH of 2–10 was adsorbed onto 0.1–0.5 g of CC-SA by shaking at 100–200 rpm for 1–24 h, at temperature of 30–50 °C. The MB adsorption process was critically monitored by withdrawing 1 mL of the Mb solution at each time interval. The un-adsorbed MB in the solution is UV–Vis spectroscopic measured at a wavelength of 665 nm using UVD-3500 (Labmoed) UV–Visible spectrophotometer. The percentage of adsorbed MB was calculated followed equation (1)

$$\% \; MB \; adsorption = \frac{C_o - C_e}{C_o} \; x \; 100 \; (\%) \tag{1}$$

where, C_o is the starting concentration of the adsorbate (mg L^{-1}); C_e is the equilibrium concentration of the adsorbate (mg L^{-1}).

2.6. Characterizations of CCA beads

All products, including the cellulose, chitosan, CC and CC-SA beads were characterized their properties, accordingly, utilizing the X-ray diffractometry (XRD), Fourier-transform infrared spectroscopy (FT-IR), scanning electron microscopy (SEM), specific surface area analysis with Brunauer–Emmett–Teller (BET) method, and Thermogravimetric analysis (TGA). Firstly, the XRD was performed on an Empyrean (PANalytical), with an X-ray diffractometer using Cu Kα radiation generated at 40 kV and 30 mA (λ = 0.154056 nm). The dried samples are spread out onto a quartz substrate and analyzed from 5 to 60° (2θ) at a scan speed of 0.6°/min. Then, the FT-IR spectra were obtained using a MIR/NIR Frontier (PerkinElmer) spectrophotometer (frequency range from 4000 to 500 cm^{-1}) with KBr pellet method. Analyses were conducted under a dry air purge at co-addition of 256 interferograms collected at 4.0 cm^{-1} resolution. The bead morphologies are also taken on a S-4800 Ultra-High-Resolution FE-SEM (Hitachi High technologies) scanning electron microscope operated at accelerating voltages of 15 kV. The samples are grounded and dropped onto the carbon-coated 300-mesh copper grids, coated with platinum, and subjected to SEM analysis in the nitrogen atmosphere. Next, the surface area and pore size distribution of the samples are taken on a BET-201A (Porous Materials Inc., USA). Sequently, thermogravimetric analysis is analyzed on thermal analysis system TGA-DSC 3+ (Mettler Toledo) in the temperature range of 25–700 °C with temperature increasing speed of 5 °C/min in nitrogen atmosphere. Finally, the surface charge of the beads is determined by using a method proved by Čerovic'et al. [22]. To this end, 0.2 g of CC-SA was placed into 25 mL of KCl 0.1 M solution in different pH values of 2, 4, 6, 8 and 10 for 24 h. The final pH was determined using a pH meter (ST3100-F, Ohaus). Finally, the surface charge of CC-SA beads was determined using the delta pH versus initial pH plot.

2.7. Isotherm and kinetics of MB adsorption

Three isotherm models, including the Langmuir model, the Freundlich, the Dubinin – Radushkevich (D-R) model and intraparticle diffusion model, were utilized for the MB adsorption.

The Langmuir isotherm adsorption equation is written as Eq. (2) [23]:

$$\frac{q_e}{q_m} = \theta = \frac{K_L C_e}{1 + K_L C_e} \tag{2}$$

where q_e represents the equilibrium adsorption capacity (mg g^{-1}), q_m is the maximum adsorption capacity (mg g^{-1}), θ is the coverage, C_e denotes the concentration of the adsorbed material as sampling (mg L^{-1}), and K_L is the Langmuir constant.

The Freundlich isotherm adsorption equation is described as Eq. (3) [24]:

$$q_e = k_F \cdot C_e^{1/n} \tag{3}$$

where q_e represents the equilibrium adsorption capacity (mg g^{-1}), K_F is the Freundlich constant or maximum absorption capacity (mg g^{-1}), n is the correction factor, C_e denotes the concentration of the adsorbed material as sampling (mg L^{-1}).

By plotting the linear form of Eq. (3), $\log q = 1/n \, \log C + \log K_F$, the slope is the value of $1/n$, and the intercept is equal to $\log K_F$.

The Dubinin-Radushkevich (D-R) isotherm model (Eq. (4)) is an empirical model used to evaluate the adsorption process's nature (physical or chemical) [25].

$$ln \; q_e = ln \; q_m - \; \beta \varepsilon^2 \tag{4}$$

where q_e represents the equilibrium adsorption capacity (mg g^{-1}), q_m is the maximum adsorption capacity (mg g^{-1}), β is the adsorption energy constant, $\varepsilon = RTln\left(1 + \frac{1}{C_e}\right)$ is Polanyi potential energy.
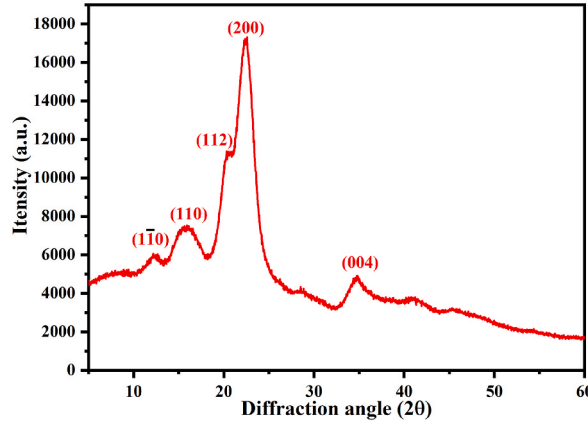
Fig. 1. X-ray diffraction (XRD) pattern of cellulose from sugarcane bagasse.

The average adsorption energy, E (kJ mol^{-1}), may be derived from D-R using the following parameter, Eq. (5):

$$E = \frac{1}{\sqrt{2\beta}} \tag{5}$$

The nature of the adsorption process is assessed by the average adsorption energy (E) value. When the E value is less than 8 kJ mol^{-1}, the process is physical adsorption, while chemical adsorption occurs when the E value is between 8 and 16 kJ mol^{-1}.

Regarding the kinetics of MB adsorption, three kinetic models are employed to estimate the apparent speed constants, the apparent kinematics of pseudo first-order (PFO), Eq. (6), and the apparent kinematics of pseudo second-order (PSO), Eq. (7).

$$ln(q_e - q_t) = ln\,(q_e) - k_1 t \tag{6}$$

$$\frac{t}{q_t} = \frac{1}{k_2 q_e^2} + \frac{t}{q_e} \tag{7}$$

where q_e represents the adsorption dynamics at equilibrium time (mg g^{-1}), q_t is the adsorption dynamics at time t (mg g^{-1}), k_1, k_2 is the apparent first-order and second-order adsorption rate constant, respectively.

The intraparticle diffusion (IPD) model proposed by Weber and Morris [26] has been widely utilized for the analysis of adsorption kinetics (Eq. (8)), and Wu et al. [27] applied the IDP model to evaluate the initial adsorption mechanism (Eq. (9) and Eq. (10)).

$$q_t = k_i t^{1/2} + C \tag{8}$$

where q_t represents the adsorption capacity at time t (mg g^{-1}), k_i is the intraparticle diffusion rate constant (mg g^{-1} min$^{-1/2}$), and C is a constant for any experiment (mg g^{-1}).

$$R_i = k_i t_{ref}^{1/2} \Big/ q_{ref} \tag{9}$$

$$R_i = \frac{q_{ref} - C}{q_{ref}} = 1 - \left(\frac{C}{q_{ref}}\right) \tag{10}$$

where t_{ref} is the longest time in adsorption process (min), q_{ref} represents the solid phase concentration at time t_{ref} (mg g^{-1}), and R_i is the initial adsorption factor of the IPD model.

2.8. CC-SA adsorbent recycling study

The CC-SA adsorbent recycling profile was investigated by evaluating desorption process using the shaking method. Briefly, the CC-SA beads were dispersed in 100 mL of a 1/3 NaCl/Ethanol cosolvent (vol/vol) and continuously shaken at 200 rpm at ambient temperature for 1 h. The adsorption and desorption of MB using CC-SA beads were repeated for 5 times to assess the recycling of the adsorbent.

Table 1
Effect of NaOH concentration and reaction time to DDA.

NaOH concentration (%)	Reaction time (min)	DDA (%)
40	90	92.56 ± 1.14
40	120	93.76 ± 0.57
40	150	95.78 ± 3.42
45	90	94.17 ± 1.14
45	120	95.37 ± 2.84
45	150	96.18 ± 2.85
50	90	94.97 ± 0.05
50	120	96.18 ± 0.57

3. Results and discussion

3.1. Recovery of cellulose from sugarcane baggage

Sugarcane bagasse, after being pre-treated to remove impurities, was processed to remove sugar, lignin, and hemicellulose. The obtained product was dried to constant mass and weighed to determine the amount of cellulose recovered. The mass of obtained cellulose was 6.51 g, accounting for 26 ± 0.57 % of the original bagasse. This result was consistent with the content of cellulose in bagasse published by Homagai et al., in 2010 [28]. However, the yield was still not high compared to the study of Sun et al. [29], in the study of Sun et al., the cellulose recovered by 10 % NaOH was 44.2 %. The reason for the low yield of recovery in this study compared to that in the study of Sun et al. may be the broken cellulose chains in the process of performing the decolorization experiment with 2 % NaClO for 3 h at 50 °C. In addition, the use of hexane solvent for extraction for 4 h at 80 °C dissolved several short-chain celluloses due to breakage in the pre-treatments. Both above processes are responsible for the decrease in cellulose recovery.

The X-ray diffraction of cellulose is determined and presented in Fig. 1, and from this the average crystal size was calculated by Eq. (11):

$$d = \frac{k.\lambda}{\beta.cos\ cos\ (\Theta)} \tag{11}$$

where, k is a constant; λ is the X-ray wavelength; β is the peak foot width (radian); θ is the angle of the peak; and d is the crystal diameter (nm).

Fig. 1 shows that the crystallization index of the cellulose sample in this study was 66.5 %, the results show the efficiency of the mechanical treatment process combined with chemical treatment such as hydrolysis, alkalinity, acid, and bleach. Some of the processing steps used in this study were like those of Kittaya et al. [30]. However, the calculated crystallinity of this study was 66.5 %, which was small compared with 71.2 % of the study of Kittaya et al., possibly due to the concentration of NaOH in the study. The NaOH concentration of 10 % showed efficiency in removing lignin cyclic compounds compared with Kittaya's 4 % NaOH concentration. However, with the same concentration of H_2SO_4 but a smaller crystallization index due to the influence of the high H_2O_2 oxidizing agent causing the removal of the double bonds and complex chains of lignin, the amorphous region of hemicellulose was removed more compared with 2 % NaClO. Besides, the results of Ali Alghooneh et al. [31] showed that the combination of alkaline treatment with some solvents such as ethanol or methanol also helped to remove lignin, increasing the purity of cellulose.

In Fig. 1, the amorphous cellulose region is shown in the low diffraction region at position 2θ = 18°, some peaks characteristic for cellulose 16°, 22.5° and 34.8° were characteristic of the crystal plane (110), (200) and (004), these crystal planes were typical for cellulose I [32,33]. However, a small peak at position 2θ = 12.2° characteristic of the plane (1 $\overline{1}$0) and a peak at 2θ = 20.5° representing the plane (110) occurred [34]. As reported by French [33], the appearance of these two peaks was typical for cellulose II. This showed that the treatment with NaOH caused the cellulose sample to be on the transition from cellulose Iβ to cellulose II. If under different conditions of temperature and alkali concentration (from 12.5 to 17 %), the conversion of cellulose I to cellulose II was an irreversible reaction [33,35].

3.2. Recovery of chitosan from shrimp shells

To recover chitosan from shrimp shells, chitin was removed protein through electrolysis. From Table 1, the DDA of chitosan was quite high, all over 90 %. The DDA value of chitosan was highly dependent on NaOH concentration and reaction time. NaOH concentration and deacetylation time accelerated DDA because the -NHCOCH₃ group present in chitin converted to -NH₂ group to form compatible chitosan [36]. However, the deacetylation become more difficult to perform as extending the reaction time; this was consistent with studies of Hossain et al. [37] and Pakizeh et al. [38]. In the same time period of 120 min, the ability to reduce acetyl group of chitin in 50 % NaOH solution reached the highest DDA at 96.18 ± 0.57 % and followed by in 45 % NaOH solution with DDA of 95.37 ± 2.84 %. Although the deacetylation increased when the concentration of NaOH solution increased, it was very small. This was because the acetyl group of chitin formed stable complexes with proteins in shrimp shells, making it difficult to separate [39]. In addition, the degree of deacetylation of chitin was influenced by the interference of chitin's steric structure [40]. Furthermore, the diffusion rate of -OH to the surface and interior of chitin were strongly dependent on the alkali concentration. Therefore, increasing the
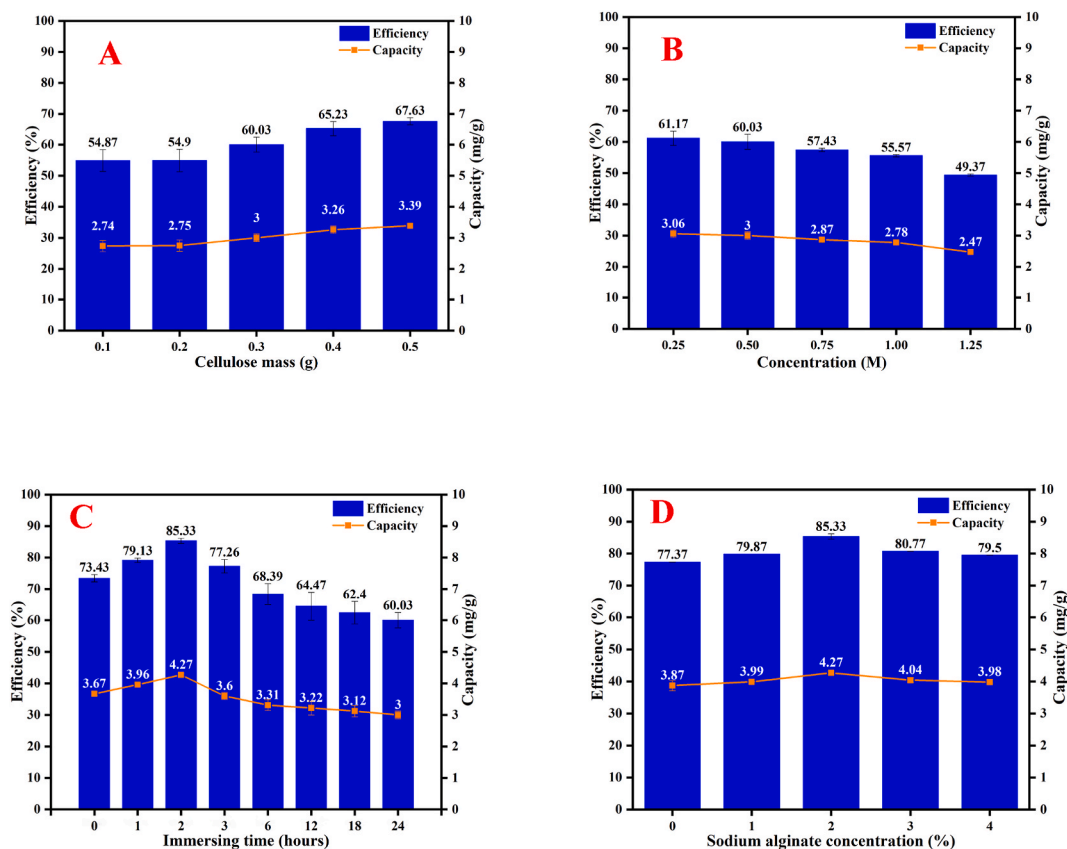
Fig. 2. Effects of cellulose mass (A), NaOH concentration (B), immersing time (C), and SA concentration (D) on MB adsorption at $C_0 = 10$ ppm, $m_{bead} = 0.2$ g, shaking speed = 100 rpm, T = 30 °C, V = 100 mL, t = 24 h.

concentration of NaOH created favorable conditions for -OH to solve the obstacle of the spatial structure, thereby increasing the degree of DDA when increasing the concentration of NaOH. If comparing the DDA value in 45 % NaOH solution, at 90 min, the efficiency was 94.17 ± 1.14 %, only 1.2 % smaller than 120 min. Therefore, 45 % NaOH solution and 90 min electrolysis time were selected as optimal conditions.

3.3. Synthesis of CC-SA beads

The results from Fig. S2 show that the mass of cellulose influenced the granulation process of the material. Solutions contenting cellulose greater than 0.3 g did not form complete globules, making the droplets mechanically weak to withstand the impact and resistance encountered when entering the granulation solution [41]. These droplets were broken or stretched, producing irregularly shaped beads as in Figs. S2D and S2E. In contrast, when cellulose mass was equal to or smaller 0.3 g, the particles formed are close to the complete sphere as shown in Fig. S2A, S2B and S2C.

Besides the particle shape, the ability to remove MB in the solution is an important factor to select the appropriate cellulose mass. MB adsorption using CC-SA beads with different cellulose contents were evaluated and presented in Fig. 2A. The results in Fig. 2A show that when changing the cellulose content in the beads, it affected the removal of MB. Specifically, MB adsorption efficiency increased from 54.87 to 54.9, 60.03, 65.23 and 67.63 % when the cellulose mass rose from 0.1 to 0.2, 0.3, 0.4 and 0.5 g, respectively. It could state that cellulose influenced the ability to remove MB based on the molecular structure of cellulose. On each link of cellulose, there were 3 -OH groups to facilitate the swelling of the material, because -OH created hydrogen bonds with water molecules in the solution, allowing MB to contact the -NH$_2$ group that had not been protonated [42]. Besides, the electron-rich oxygen of the -OH group can form an electrostatic attraction with MB, enhancing the adsorption capacity for MB [43]. This indicated that cellulose not only acted as a filler, but also had the ability to adsorb when under the right conditions. From the above basis, the mass of cellulose was chosen as 0.3 g to investigate other factors due to the uniform spherical size of the material particles and the relative MB adsorption efficiency.

NaOH solution was selected as the solvent to make CC-SA beads. The process of CC-SA particle formation is called phase inversion, that is, the change from the gel phase of chitosan back to the original solid phase by modifying the glycosidic bonds [44]. CC-SA beads were shaped through two processes: gelation and precipitation. This chitosan precipitation process was an acid-base reaction. Chitosan was dissolved in 2 % acetic acid solution; the acidic medium was responsible for protonation. The amine groups (-NH$_2$) of each link on
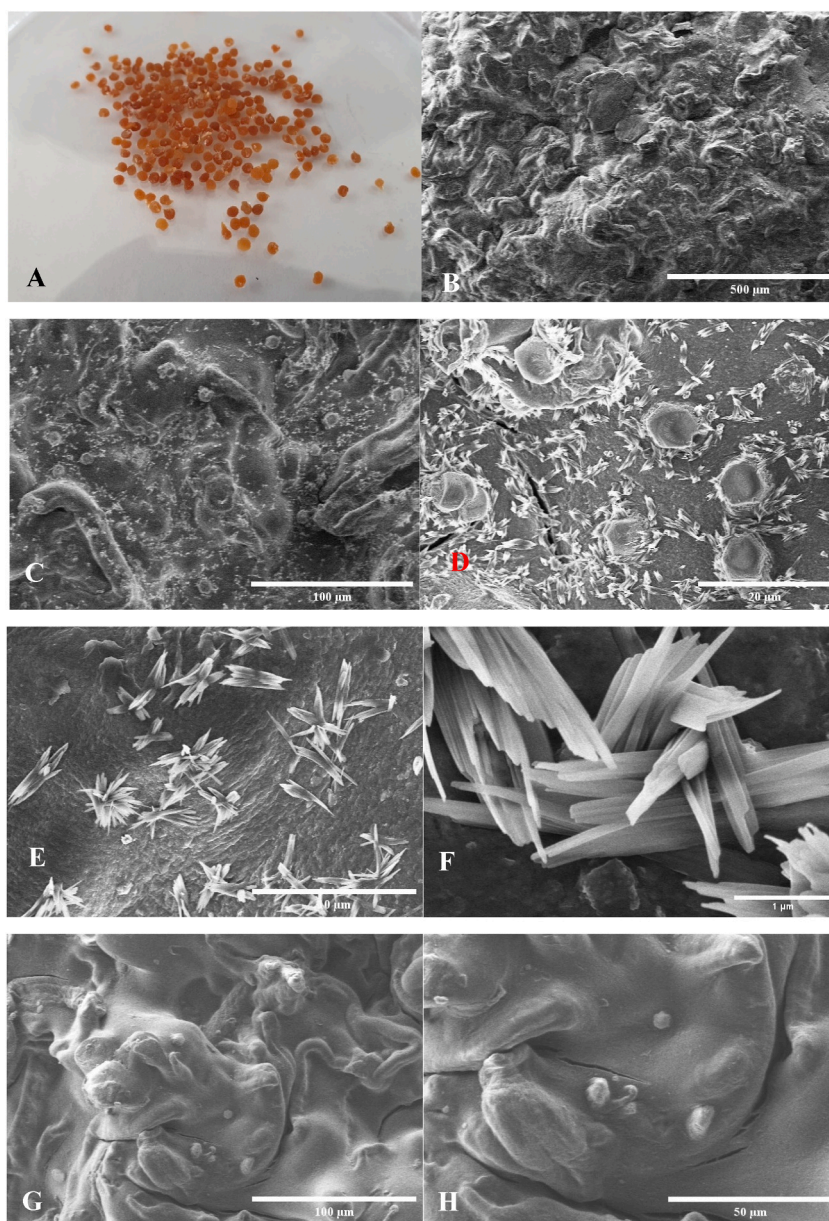
Fig. 3. Digital image of CC-SA (A), SEM images of CC-SA at different magnification x100 (B), x500 (C), x2000 (D), x5000 (E), x30000 (F), and SEM image of CC at different magnification x500 (G), x1000(H). Condition: Accelerating Voltage: 5000 V, WD = 8 mm.

the chitosan molecule accepted protons and converted them to a positively charged cation group (NH_3^+), making the cationic chitosan polymer become more polar, so it was completely soluble in water. The precipitation process was done by NaOH solution, when dropping the cellulose/chitosan mixture (CC) into the NaOH solution on the contact surface between the droplet and the NaOH solution was neutralized the groups (NH_3^+) by –OH, making it less polar. Therefore, chitosan was rapidly precipitated on the surface of cellulose, when the chitosan polymer chains in contact with NaOH caused an increase in the surface viscosity to form a gel layer covering the CC. The second stage due to excess –OH caused the surface to change from gelation to precipitate [44]. The increase in the concentration of NaOH solution contributed to the faster and more stable precipitation process, so the obtained particles had uniform size as well as the surface was quite stable compared to dripping into NaOH solution with lower concentration (Fig. S2F., S2G, S2H, S2I and S2J). On the contrary, when the concentration of NaOH was too high, the large number of anions neutralized the cations on the surface of the particles, affecting the electrostatic force when immersed in sodium alginate solution, reducing the adsorption capacity. Specifically, the MB adsorption efficiency of the CC-SA beads soaked at different concentrations of NaOH was presented in Fig. 2B as follows: When the concentration of NaOH was 1.25 M, the bead formation process took place quickly and efficiently. The adsorption capacity of particles was limited to only 49.37 ± 1.08 %. When the concentration of NaOH gradually decreased, the MB adsorption
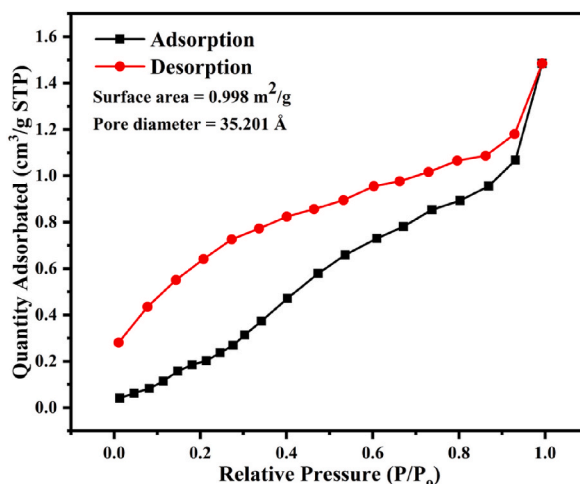
Fig. 4. Nitrogen adsorption/desorption isotherm of CC-SA beads at 77 K.

efficiency increased gradually. At two concentrations of NaOH, 0.25 M and 0.5 M, the adsorption results were similar, however, the beads at 0.5 M NaOH concentration produced uniform and more stable particles than those at NaOH concentration 0.25 M. Therefore, the concentration of 0.5 M NaOH was chosen as a condition for particle synthesis for further investigations.

Fig. 2C shows the influence of the immersing time the CC-SA beads in 0.5 M NaOH solution. When increasing the immersing time, the adsorption efficiency increased in the first 2 h and then decreased in the following hours. Based on the adsorption results, when immersing time was in 2 h, the adsorption efficiency was 85.33 ± 0.85 %. When immersing time increased from 3 to 24 h, the adsorption efficiency decreased from 77.26 ± 2.14 % to 60.03 ± 2.4 %. It is shown that increasing the immersing time reduced the adsorption efficiency, attributing to cross-links between amine groups of chitosan and hydroxide groups of cellulose causing reduce porous structure of the beads [21]. From the above results, the optimal time to immerse the CC-SA beads in the NaOH solution was 2 h.

CC-SA material particles were covered by sodium alginate (SA) layer, so the concentration of SA affected the particle strength as well as the adsorption capacity. The main interaction of this material was electrostatic interaction, so the high concentration of SA could give better results of adsorption investigation. Therefore, the effect of SA concentration on MB adsorption capacity was investigated and presented in Fig. 2D. The results from Fig. 2D indicated that the coating of alginate on the surface did not significantly affect the adsorption capacity of CC-SA beads. The CC material particles achieved the adsorption efficiency of 77.37 ± 3.15 %, while the CC-SA particles achieved the adsorption efficiency of 85.33 ± 0.85 % when the material particles were soaked in 2 % sodium alginate solution, the adsorption capacity increased by only 8 %. However, this coating helped to protect the surface of the material and still worked well under acidic conditions (pH 2.0) as in Fig. 10b and c. Therefore, the optimal condition for soaking the CC beads in SA solution was 2 %.

3.4. Characterizations of CC-SA beads

Digital images and scanning electron microscopy of CC-SA beads were used to evaluate the surface morphology of the material and the results were presented in Fig. 3. It can be seen that the material was shrunk after drying to constant weight [16]. The size of the beads was determined using a digital ruler, the fabricated beads were quite uniform in size with an average diameter of 1.57 ± 0.12 mm as in Fig. 3A. In addition, CC-SA beads had a fairly complete spherical shape, which was similar to the study of Qin et al. [45]. The surface of CC-SA beads was rough as captured by a scanning electron microscope (Fig. 3B). Therefore, to clarify this problem, the SEM image of the bead with a magnification of x500 (Fig. 3C) was taken and the results showed that the outer surface of the material has many slots, convex and convex blocks with size fluctuations of a few tens of micrometers, predicting that the bead could create many adsorption sites [46]. In Fig. 3C, D and 3E, the white flakes on the bead surface can be attributed to SA adhering to the bead surface after the coating process. Comparing to the surface of the bead without SA coating in Fig. 3G and H, Fig. 3F with a magnification of x20, 000 can clearly observe the SA fragments forming on the surface of the beads. It can conclude that SA is successfully coated on the grain surface. Besides, Fig. 3D showed that the surface of the bead possessed a certain pore with slit shape, and this could be the main way for MB solution to penetrate inside CC-SA beads.

The specific surface area of the material was determined by the adsorption isotherm according to the BET (Brunauer-Emmett-Teller) theory to determine not only the surface area but also the volume and pore diameter through the process of adsorption-desorption isotherm with N_2 gas at 77 K. Fig. 4 shows that the desorption capacity of the material is better than that of adsorption. Through the measured data, the surface area of the material is $0.998 \text{ m}^2 \text{ g}^{-1}$, compared with some other studies [41,45,46], the CC-SA composites had a much smaller surface area due to the peculiarity of the bead shape and drying at 60 °C for a long time, causing the bead to shrink and collapse its original structure, then making the pore diameter smaller. The average pore diameter was 3.52 nm, thus the beads belonged to the mesoporous type with the size from 2 to 50 nm [47]. The adsorption isotherms classification is characteristic
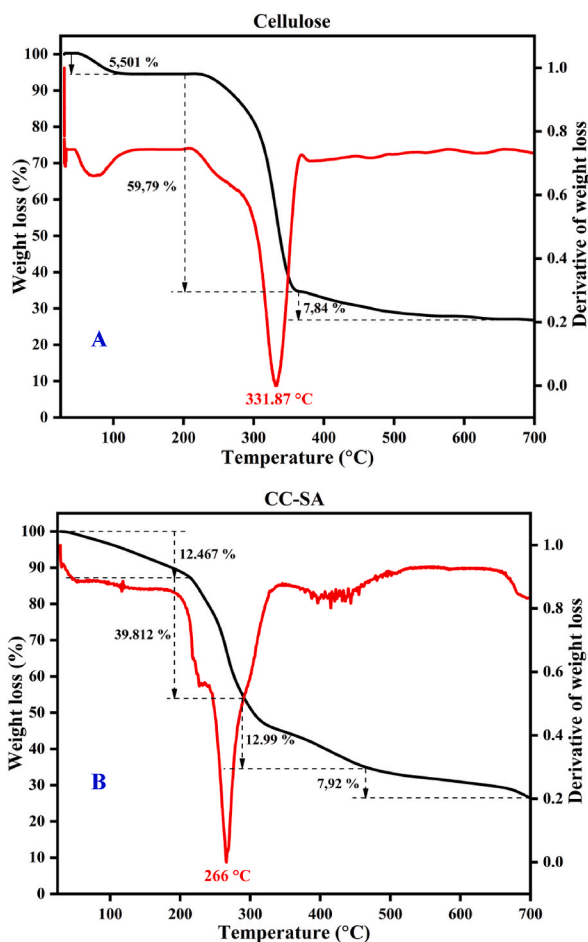
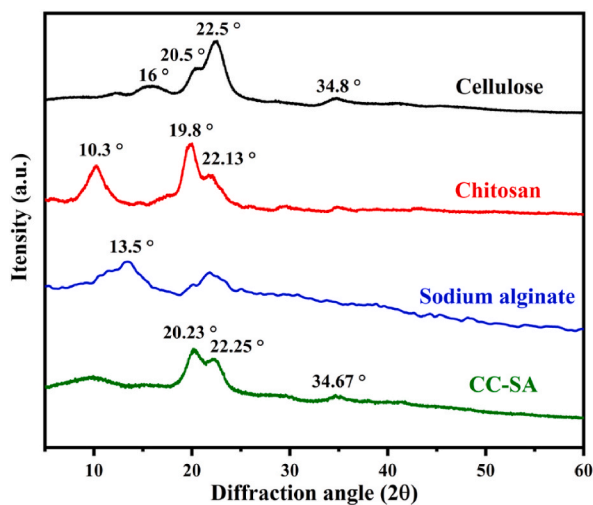**Fig. 5.** TGA and DTG of cellulose (A) and CC-SA (B).

Fig. 6. X-ray diffraction pattern of cellulose, chitosan, sodium alginate and CC-SA.

of adsorbents divided into six types including microporous (type I), nonporous or macroporous (types II, III, and VI), or mesoporous (types IV and V). Type V indicated that the adsorbents owned a certain pore with a slit shape, and the adsorbate-adsorbent interaction was weak [48]. This description was in good agreement with the observation based on SEM images of CC-SA beads in Fig. 3.
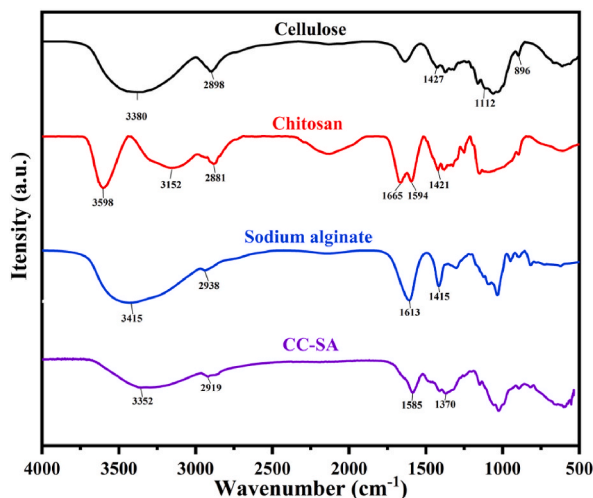
Fig. 7. FT-IR spectra of cellulose, chitosan, sodium alginate and CC-SA.

Furthermore, due to the mesoporous structure, the CC-SA can simply adsorb MB molecules, possessing a length of 13.82 Å to 14.47 Å and a width of about 9.5 Å [49]. Because the diameter of CC-SA beads was larger and the pore network distributing from large to small in the direction from the outside to the inside of the bead, to achieve high adsorption efficiency, it can take a long time for MB molecules to diffuse into the capillary pore.

Cellulose after being recovered from sugarcane bagasse by mechanical method, hydrolyzed by acid, treated with NaOH and bleached, was evaluated for thermal stability through weight change with temperature by TGA and DTG charts in Fig. 5. TGA results of cellulose showed that the mass change of cellulose was divided into two different stages as in Fig. 5A. Stage 1 at a temperature range of 50–125 °C, the 5.5 % mass loss at this stage was caused by the evaporation of physical water in the sample. In stage 2, the sample mass was reduced by 59.78 % from the initial mass in temperature range from 230 to 375 °C, this was due to the decomposition of hemicellulose at 220 °C and degradation of cellulose taken place at around 315 °C [50]. Through the DTG curve, the decomposition temperature of the cellulose in this study was at 331.87 °C, being higher the previous report [50], attributed to high purity of the cellulose sample in this study [51]. Thus, the recovered cellulose in this study was of high purity.

For the CC-SA material sample (Fig. 5B), the TGA curve represented four different stages of mass loss. In stage 1, the mass loss was 12.47 % in the temperature range of 25–213 °C due to evaporation of the physical water in the sample. Phase 2 from 213 to 313 °C, thanks to the destruction of glycoside bonds of SA corresponding to chain break of the SA chain [52] and the decomposition of the polymer chains of chitosan [53], the sample mass reduced 39.81 %. Stage 3 from 313 to 465 °C, the mass reduced 12.99 % because of the decomposition of cellulose at 315 °C [50]. Stage 4 from 465 to 700 °C, the mass loss was due to the conversion of SA into Na_2CO_3 [52,54].

The X-ray diffraction patterns of cellulose, chitosan, sodium alginate were illustrated in Fig. 6. For cellulose, some characteristic peaks of cellulose observed at positions $2\theta = 16°$, $18°$, $22.5°$ and $34.8°$ were typical for cellulose I [32,33]. Besides, a small peak appeared at position $2\theta = 12.2°$ and a peak at $2\theta = 20.5°$ appeared, and these two peaks were typical for cellulose II [33,34]. This indicated that the treatment with 10 % NaOH caused the transition from cellulose Iβ to cellulose II in the cellulose sample. For the XRD spectrum of chitosan, this semi-crystalline polymer was observed with the appearance of 2 characteristic peaks at positions $2\theta = 10.3°$ and $19.8°$, as well as a small peak with low intensity of $2\theta = 22.13°$ [55–57]. This semi-crystalline nature was attributed to each link of the chitosan molecule carrying many O-H and N-H groups, which can form hydrogen bonds between different molecules and strongly intramolecular [56]. The diffraction peak at $2\theta = 10.3°$ was typical for the appearance of primary amines (-NH$_2$), while the position at $2\theta = 19.8°$ was for secondary amines (-N-CO-NH$_3$) [58]. For the XRD results of sodium alginate, the characteristic peak appearing at position $2\theta = 13.5°$ was typical for the crystallization region of SA [59]. Finally, the XRD of CC-SA beads from Fig. 6 indicated that the structure of the material was semi-crystalline. In fact, the diffraction double tip of cellulose and chitosan could be observed at $2\theta = 20$–$22°$, specifically 20.23° and 22.25° formed by the overlap of two peaks with lower intensity than the original cellulose and chitosan samples. This result was caused by combination of cellulose and chitosan in the CC-SA, leading to the formation of hydrogen bonds of these two components. It was observed that initially the characteristic peak of cellulose was higher than that of chitosan, but the characteristic peak of cellulose in CC-SA was lower than the characteristic peak of chitosan, this is because percentage of chitosan in CC-SA was greater than that of cellulose. Besides, the peak of SA at $2\theta = 13°$ disappeared in the CC-SA material, there were two reasons for this. Firstly, the structure of the bead was mainly amorphous region, it is difficult to detect in the material particles. Secondly, the mass ratio of SA was very small in CC-SA, the characteristic peak of SA was obscured by the characteristic peak of cellulose and chitosan, leading to undetectable.

FT-IR spectroscopy is often used to determine the presence of functional groups, or to understand the change in chemical properties of samples after treatment. In this study, the FT-IR spectra of the cellulose, chitosan, SA and CC-SA beads were presented in Fig. 7. The FT-IR results showed absorbance peaks in the wavelength range of 3589–3379 cm^{-1} corresponding to cellulose, chitosan and SA
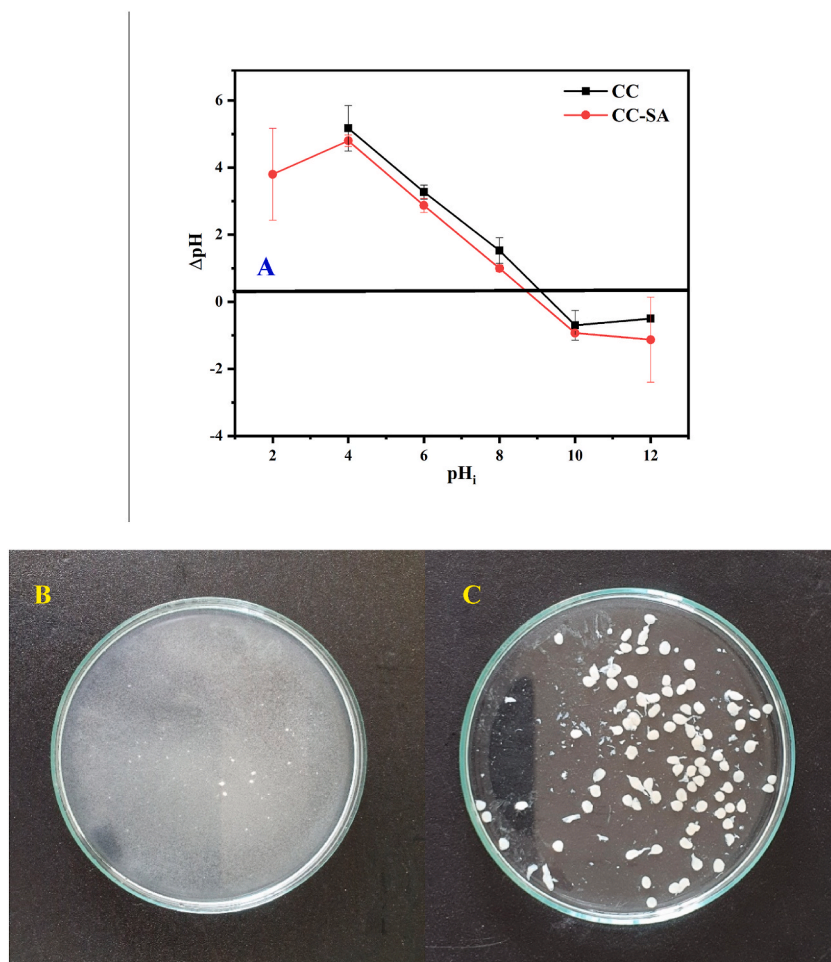
Fig. 8. pH$_{pzc}$ of CC-SA (A) and stability of CC bead (B) and CC-SA bead (C) at pH 2.0.

represented the elongation oscillation of O–H groups. The wavelength ranging from 1150 to 1034 cm^{-1} in FT-IR spectra of cellulose, chitosan and SA showed the prolonged fluctuation of C–O–C group characterizing for the polysaccharide structure. In addition, the FT-IR of each spectrum had its own characteristic peaks. For the FT-IR spectrum of cellulose, the wavelength at 2898 cm^{-1} was typical for a symmetrically stretched C–H bond, while the peak at 1427 cm^{-1} and 896 cm^{-1} characterized for the symmetric bending vibration of the –CH$_2$ group and the β-Glycoside bonds of the glucose ring of the cellulose structure [60]. For the FT-IR spectrum of chitosan, the 1665 and 1594 cm^{-1} oscillations characterized the two typical peaks of the chitosan spectrum. The wavelength of 1665 cm^{-1} characterized the primary amide group existing in each link. Meanwhile, since the process de-acetylation took place incompletely so that in the structure of chitosan still had the secondary amide group characterizing at a wavelength of 1594 cm^{-1} [61–63]. Similar to cellulose, the peak at 2881 cm^{-1} and 1421 cm^{-1} were characteristically for an elongated C–H bond and a bent C–H bond, respectively [61–63]. For the sodium alginate spectrum, the peak at 1613 cm^{-1} was typical for the extended –C=O group while the peak at 1415 cm^{-1} was attributed to the asymmetric –COOH group [64].

For FT-IR spectrum of the CC-SA bead, because it was a composite material from cellulose, chitosan and SA, its FT-IR spectrum could have characteristic peaks like the material, it is composed of. The wavelength at 3352.3 cm^{-1} was formed by the overlapping of the characteristic peaks of the O–H, N–H groups [17] and in the meantime the shift of wavelength from 3415 to 3379 cm^{-1} to 3352 cm^{-1} indicated that the hydrogen bonding of the compound was enhanced. The stretching oscillation of C–H was determined at a wavelength of 2919 cm^{-1}. However, the wavelengths at 1665 cm^{-1} and 1415 cm^{-1} characteristic for the primary amide group and the asymmetric –COO group were not found in the CC-SA bead possibly because of overlapping from the peaks of the original compounds. Meanwhile, the wavelengths moved down to the lower wavenumber from 1665 cm^{-1} to 1585 cm^{-1} and from 1415 cm^{-1} to 1369 cm^{-1}, indicated that the amino group of chitosan interacted with carboxyl group of sodium alginate [63]. In summary, the CC-SA material were formed not only by mechanical mixing but also by the formation of hydrogen bonds between the functional groups of the components making up the CC-SA.

The surface charge of the CC and CC-SA bead were evaluated and shown in Fig. 8A. It can bee seen that the change in surface charge of CC-SA bead from positive to negative with increasing pH, and the point of zero charge of CC-SA bead was determined at 9.04. The
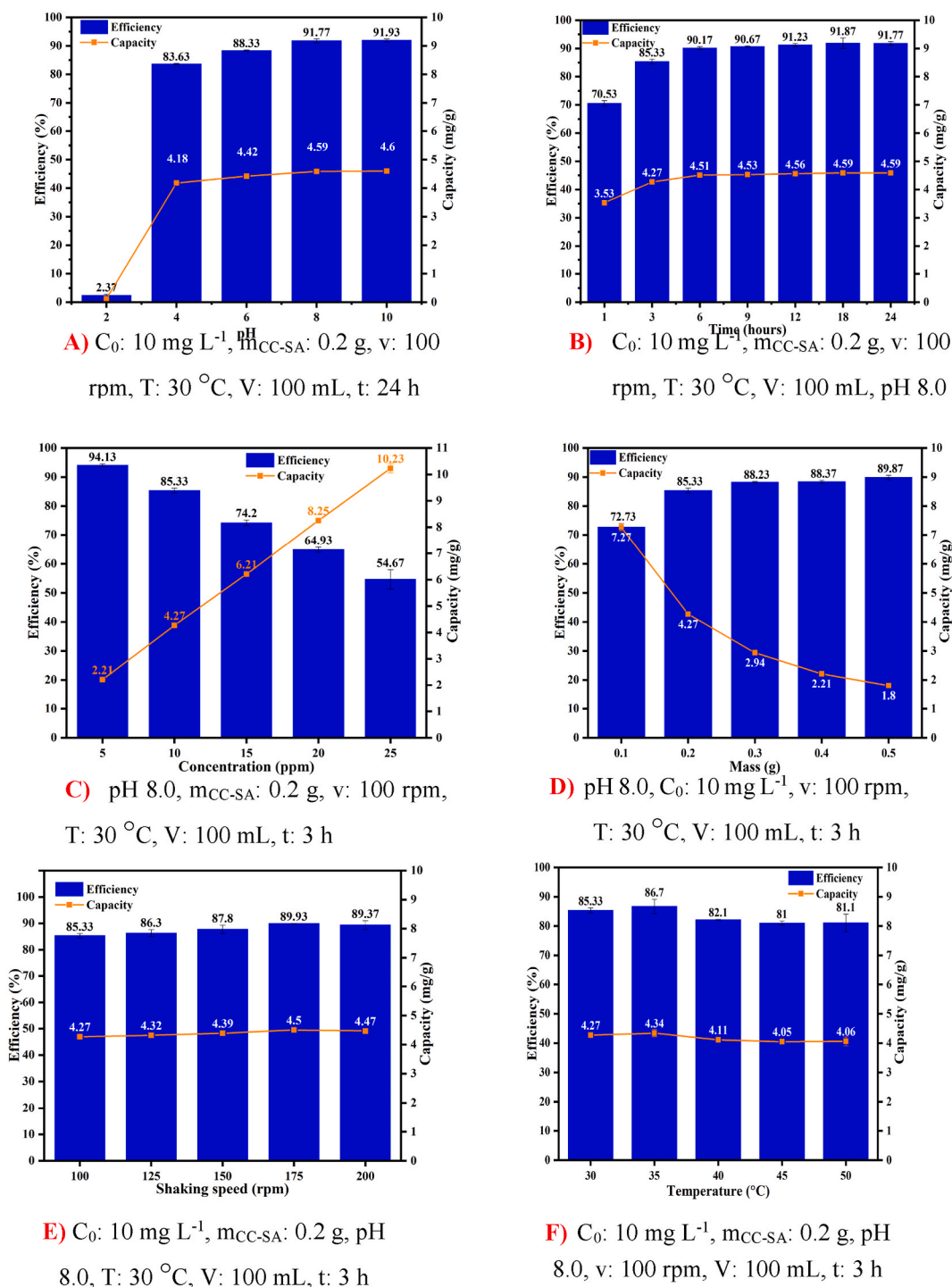
Fig. 9. Effects of pH (A), contact time (B), initial MB concentration (C), adsorbent dose (D), shaking speed (E), and temperature (F) on MB adsorption using CC-SA beads.

bead surface is positively charged when pH < 9.04 and negatively charged when pH > 9.04. Thus, it can predict that at pH < 9.04 the bead is good at adsorbing anions, at pH > 9.04 it is good at adsorbing cations. Therefore, it can state that MB^+ ions are likely to be adsorbed by the CC-SA bead when pH is greater than 9.04. In this study, it is interesting that calcium alginate crosslinking in the coated particles remains stable even at a low pH of 2 (Fig. 8C), which is remarkable as this is usually a condition where carboxylated-calcium crosslinking is compromised due to protonation. This stability suggests that the beads possess particular properties, possibly due to
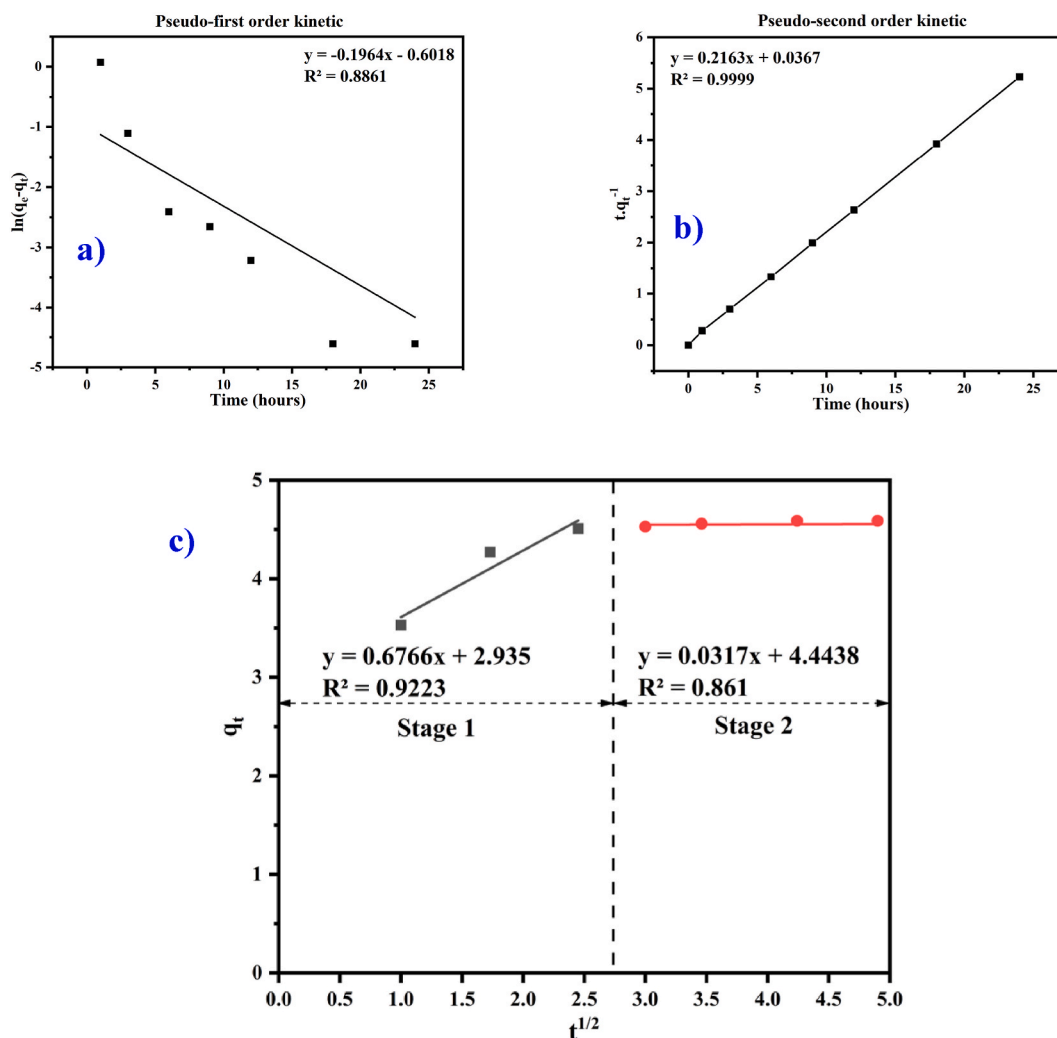
Fig. 10. Pseudo-first-order model (a), Pseudo-second-order model (b), Intra-particle diffusion model (c) for MB adsorption using CC-SA bead.

enhanced crosslinking density, the presence of stabilizing agents, or specific structural modifications. This finding is significant for applications in acidic environments, such as drug delivery systems in the stomach or industrial processes, where conventional alginate gels would typically dissolve as Fig. 8B [62].

3.5. Adsorption of MB using CC-SA beads

Several factors influence the adsorption of dyes and solution pH is one of the most important factors due to its impact on both the ionization process of the dye molecules and the active sites of the adsorbent in the solution [65]. Basically, when MB dissociated in water, it created MB^+, which was favorably adsorbed by the negative charge on the surface of CC-SA at pH greater than 9.04. The effect of pH on MB adsorption in this study was presented in Fig. 9A. Specifically, when the pH gradually increased from 2 to 10, the adsorption efficiency increased. However, at pH 2, the CC-SA beads had an insignificant adsorption of MB, the efficiency was only 2.37 %. The poor adsorption efficiency (2.37 %) at pH 2 can indeed be attributed to the competitive adsorption between H^+ ions and MB^+ ions, where H^+ ions are favored due to their smaller size and higher mobility. Furthermore, the Ca ion carboxylate crosslinking pKa is around 4–5, which suggests that at pH 2, the crosslinked structure of alginate may undergo changes that reduce its porosity. This decreased porosity at low pH likely hinders the diffusion of MB molecules into the beads, thus limiting adsorption. At pH values of 4, 6, 8 and 10, MB adsorption efficiency was 83.63 ± 0.23 %, 88.33 ± 0.25 %, 91.77 ± 0.64 % and 91.93 ± 0.49 %, respectively. As the pH increases to 4, the adsorption efficiency significantly improves. This improvement can be explained by the reduced competition from H^+ ions and a potential morphological change in the alginate structure. The crosslinking of Ca ions and alginate at this pH range (pKa around 4–5) may create a more porous structure, facilitating better diffusion and adsorption of MB molecules. The increase in porosity and the reduction in electrostatic hindrance likely contribute to the higher adsorption efficiency observed at pH 4 and above. Besides, although pH 4 was an acidic environment, the adsorption capacity of the particles was still high, proving that besides the electrostatic

Table 2

Kinetic parameters and coefficients of PFO, PSO and Intra-particle diffusion model of adsorption of MB on CC-SA bead.

Kinetic model	Parameters	Definition	Values
Pseudo-first-order	q_e, cal (mg g^{-1})	Calculated adsorption capacity	0.547
	k_1	Rate constant	0.1964
	R^2	Correlation coefficient	0.8861
Pseudo-second-order	q_e, cal (mg g^{-1})	Calculated adsorption capacity	27.59
	k_2	Rate constant	0.006
	R^2	Correlation coefficient	0.9999
Stage I	k_{p1}(mg g^{-1} min$^{-1/2}$)	Rate constant at stage 1	0.6766
	C_1	Intercept at stage 1	2.935
	Ri_1	The initial adsorption	0.9223
	R^2	Correlation coefficient	0.23
	C/Q_{ref}		0.77
	Zone		III
	Description		strong adsorption
Stage II	k_{p2}(mg g^{-1} min$^{-1/2}$)	Rate constant at stage 2	0.0317
	C_2	Intercept at stage 2	4.4438
	Ri_2	The initial adsorption	0.015
	R^2	Correlation coefficient	0.861
	C/Q_{ref}		0.985
	Zone		IV
	Description		saturated adsorption

interaction between the adsorbent and the adsorbate, the adsorption of MB onto CC-SA beads was influenced by van der Waals forces of the macromolecules making up the beads; and this attraction can compete with electrostatic force of protons in acidic environment [66]. It can be found that permissible range of pH for treated wastewater discharge was ranging from 6.0 to 9.0 [67]. Therefore, the pH 8.0 was chosen to investigate the other affecting factors of the MB adsorption by CC-SA beads.

To assess the adsorption rate, contact time effect on MB adsorption capacity using CC-SA beads was conducted and depicted in Fig. 9B. The results showed that the adsorption equilibrium in CC-SA beads obtained in the first 6 h and reached the adsorption efficiency of 90.17 ± 0.02 %. The adsorption sites were partially saturated within 1–3 h of contact and complete equilibrium was achieved after 6 h [68]. When adsorption time increased further to 24 h, the efficiency changed insignificantly, fluctuated around 91 % over the adsorption time period from 9 to 24 h. This is because the adsorption process of dye solution for porous solid materials took place in the following stages [69]. The first stage was the displacement of MB molecules from the solution to the outer surface of the adsorbent. The second and third stages involved diffusion of MB molecules across the surface of solution or solid, forming bonds between MB molecules and localized adsorption sites on the surface of the adsorbent (inner surface of the material particles). Finally, diffusion and permeation of MB molecules into the pores took place. Such diffusion was enhanced when the pores communicated with each other when beads have irregular surfaces with interconnected pores homogenously distributed throughout the matrix [68,69]. Therefore, the adsorption time of MB dye by CC-SA beads was longer than that of powder adsorbent materials. In this study, the adsorption time of 3 h was selected to investigate the influence of subsequent factors.

Initial concentration plays a critical role in the adsorption process. This study investigated the influence of initial MB concentration ranging from 5 to 25 ppm on its adsorption using CC-SA beads and the results were presented in Fig. 9C. When increasing the concentration of MB solution from 5 to 25 ppm, the adsorption efficiency decreased from 94.13 ± 0.4 % to 54.67 ± 3.3 %, but the adsorption capacity rose from 2.21 ± 0.02 mg g^{-1} to 10.23 ± 0.17 mg g^{-1}. Details were as follows: when rising the concentration of MB from 5 to 10 ppm, the efficiency decreased from 94.13 ± 0.4 % to 85.33 ± 0.85 % but the adsorption capacity increased from 2.21 ± 0.02 mg g^{-1} to 4.27 ± 0.04 mg g^{-1}. At C_0 = 15 ppm, the efficiency decreased to 74.2 ± 1.04 % but the adsorption capacity was 6.21 ± 0.06 mg g^{-1}, an increase of about 45 % compared to C_0 = 10 ppm. When MB concentration was 25 ppm, although the adsorption efficiency decreased to 54.67 ± 3.3 %, the adsorption capacity increased to 10.23 ± 0.17 mg g^{-1}, 4.6 times higher than that of MB at C_0 = 5 ppm. The solution at low concentration had fewer dye molecules than the solution with high concentration, resulting in a small concentration gradient that made the diffusion of MB dye molecules into the bead slower than in high concentration solution [66]. However, due to the low concentration of dye molecules, the adsorption efficiency of the dilute solution was higher than that of the solution with high concentration, the initial MB concentration of 10 ppm was chosen to further experiments.

In contradiction of initial concentration, increasing adsorption mass causes a growth-up of adsorption efficiency, but a reduction of adsorption capacity, so in this study, the mass of the adsorbent changed from 0.1 to 0.5 g to evaluate the influence of the CC-SA mass on MB removal efficiency, and the results was shown in Fig. 9D. When the CC-SA mass increased from 0.1 to 0.5 g, the adsorption efficiency increased from 72.73 ± 1,29 % to 89.87 ± 0.75 %. In general, increasing the CC-SA mass up to 0.5 g significantly increased the number of adsorption sites, which allowed the MB$^+$ solution to interact more with the adsorbent [68]. However, the adsorption capacity greatly reduced as the mass of adsorbent increased. Therefore, a mass of 0.2 g of adsorbent was selected for further investigations.

In this study, when changing the shaking speed, the MB adsorption efficiency almost unchanged. Fig. 9E showed that at the speed range of 100–200 rpm, the efficiency was about 85–89 %, the efficiency and capacity change was trivial, less than 5 %. In general, the results of adsorption efficiency and adsorption capacity were no difference when the shaking speed changed, which showed that changing the shaking speed did not affect the adsorption capacity of the beads. Therefore, shaking speed of 100 rpm was a fixed factor

Table 3
Isotherm parameters and coefficients of Langmuir, Freundlich, and D-R model of MB adsorption using CC-SA beads.

Adsorption isotherm	Parameters	Values
Langmuir	q_{max} (mg g^{-1})	22.83
	k_L (L mg^{-1})	0.1774
	R^2	0.8801
Freundlich	k_F (L mg^{-1})	1.794
	$1/n$	0.1618
	R^2	0.9498
Dubinin- Radushkevich	E (kJ mol^{-1})	0.820
	R^2	0.9498

for studying the influence of the next factor in this work.

In this study, the influence of temperature on MB adsorption using CC-SA bead was evaluated and presented in Fig. 9F. The adsorption capacity of CC-SA adsorbent decreased by 4 % when the temperature changed from 35 to 50 °C and the capacity value decreased steadily with temperature. This result showed the practical applicability of the CC-SA bead in the removal of MB$^+$ under regular conditions. The value of adsorption capacity decreased with increasing temperature, which can be explained by three main reasons: (i) high temperature increased the solubility of MB and prevented the possibility of interaction between dye solution – adsorbent material; (ii) the interaction between adsorbate and adsorbent was weakened due to the high kinetic energy of the components participating in the adsorption process; and (iii) the mobility of MB molecules in solution increased and affected their adsorption [68–70].

3.6. Adsorption kinetic, isotherm and thermodynamic of MB adsorption using CC-SA beads

Adsorption kinetic models are used to control the mechanism providing suitable data to improve the adsorption capacity and feasibility of scale-up. In this study, the mechanism of MB adsorption using CC-SA bead was studied by fitting PFO and PSO to the experimental data. The results and the important parameters were shown in Figs. 10A and B and Table 2, respectively. The results showed that the linear regression coefficient (R^2) of PFO equation was 0.8661 and q_e was 0.547 mg g^{-1}, lower than experimental one, showing that the MB adsorption process of CC-SA bead according to PSO adsorption kinetics was not suitable. Meanwhile, the R^2 of PSO equation was at 0.9999 and the q_e was at 27.59 mg g^{-1}, which indicated that the MB adsorption of CC-SA bead followed the PSO kinetic model. The applicability of PSO model to describe the MB adsorption kinetics was also stated by Jia et al. [49] via bone char and by Kumar et al. [71] with sulfuric acid-treated orange peel.

In this study, since the adsorbent is bead, it is needed to hire an intra-particle diffusion (IPD) model to investigate and the results were presented in Fig. 10C and Table 2. According to the model of IPD, the MB adsorption process on the surface of the adsorbent underwent two stages: stage I (from the beginning of adsorption to 6 h) with parameters: rate constant degree ($K_1 = 0.6766$), correlation coefficient ($R^2 = 0.9223$), ratio between the initial and maximum amount of adsorption in the period ($C/Q_{ref} = 0.77$), this was the adsorption phase which strongly belongs to zone III according to study Wu et al. [27]. Stage I included the interaction of the MB$^+$ ions with the available adsorption sites on the phase separation surface, the main force in this process was the electrostatic force due to the -OH group (cellulose), NH_2/NH_3^+ (chitosan) and –COO- (sodium alginate) and van der Waals forces due to long chain macromolecules of cellulose chains and chitosan. In addition, this stage included diffusion of MB molecules to the liquid surrounding the particle, MB adsorption on adsorption centers, and diffusion of dye molecules through pores of different sizes [72]. Stage II (from 9 h to 24 h) with parameters: rate constant ($K_2 = 0.0317$), correlation coefficient ($R^2 = 0.861$), ratio of initial and final adsorption amounts ($C/Q_{ref} = 0.985$) was typical for zone IV. This was the equilibrium adsorption stage due to the C/Q_{ref} ratio closed to 1, showing that the adsorption capacity at this stage did not change significantly (below 5 %), also exhibiting the ability to slowly diffuse dye molecules into the pores, which was proved by the pore diameter and surface area in the analysis of the specific surface area of CC-SA beads (Figs. 3 and 4). The intercept values ($C \neq 0$) suggested that intra-particle diffusion was not the only rate-limiting step, but also thanks to other adsorption mechanisms [73]. Therefore, stage II was the rate-limiting step of MB adsorption process using CC-SA beads.

The adsorption capacity of adsorbents is typically assessed by employing adsorption isotherms. These isotherm equations define adsorbent and adsorbate interaction, and the surface properties of adsorbent as well [74]. In this study, the experimental data were fitted to the Langmuir and Freundlich adsorption isotherm model. According to Eq. (2), the nonlinear Langmuir model was depicted in Fig. S3A and the Langmuir constants k_L (L g^{-1}) and q_{max} (mg g^{-1}) were shown in Table 3. It can see that the maximum adsorption capacity of 22.83 mg g^{-1} was calculated at 303 K with $R^2 = 0.8801$. Nevertheless, the regression coefficient was a slight far from 1, indicating that experimental data were not entirely in good agreement with the Langmuir adsorption isotherm.

The Freundlich adsorption isotherm model pretended multilayer coverage on the surface of the adsorbent and surface heterogeneity [24]. In this study, Fig. S3B and Table 3 showed the nonlinear Freundlich model, the isotherm constants and coefficients calculated from the linearized model. Table 3 indicated a high regression coefficient, $R^2 = 0.9498$, implying that the MB adsorption by CC-SA beads was more reliable with the Freundlich model than the Langmuir one. For the Freundlich model, as $1/n = 0.1618$, the adsorption process was favorable due to the low slope of the straight line. Moreover, the adsorption of MB using CC-SA adsorbent was reversible process with multilayer adsorption and different adsorption energy between adsorbate and adsorbent [73].

The Dubinin-Radushkevich (D-R) model was useful to study the adsorption free energy and characteristic porosity [75], and

Table 4
Thermodynamics associated with MB adsorption on CC-SA beads.

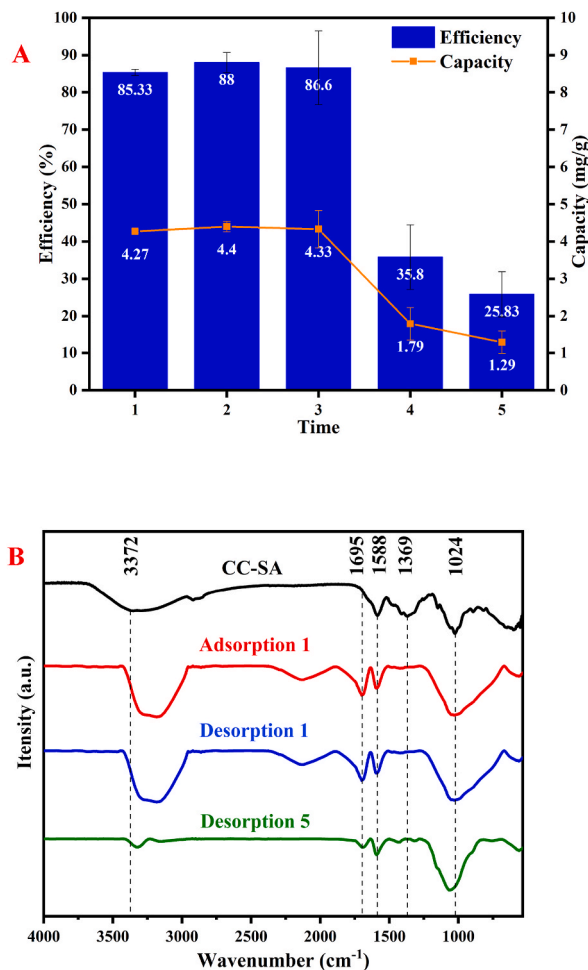| Parameter	30 °C	35 °C	40 °C	45 °C	50 °C
ΔH (kJ/mol)			0.1028		
ΔS (J/mol)			15.97		
ΔG (J/mol)	−4736.5	−4816.3	−4896.2	−4976	−5055.9

Fig. 11. Regeneration (A) and FT-IR of fresh and spent CC-SA (B).

temperature dependent, indicating the heterogeneous surface of the adsorbent [54]. This work utilized Eq. (4) to scheme D–R chart in Fig. S3C. The mean free energy was determined to be E = 0.820 kJ mol^{-1}, which was smaller than 8.0 kJ mol^{-1}, the adsorption type can be described by physical interaction [25]. In this work, the regression coefficient (R^2) of D-R model is 0.9498, indicating that the experimental data highly agreed with the D-R model. Consequently, MB adsorption onto the surface of CC-SA bead was well described by both Freundlich and D-R adsorption isotherm model.

The plot of ln(K) versus 1/T leads to values of ΔH and ΔS and the results are given in Table 4 [76]. The value of ΔS is greater than zero, showing that the dye molecules are condensed on surface of adsorbent. In addition, all values of ΔG at different temperatures are negative, which stands for a spontaneous adsorption occurred between Mb and CC-SA beads.

3.7. CC-SA adsorbent recycling study

In order to increase the applicability of CC-SA material to practical dye treatment, the reusability of the material was shown in Fig. 11A. In the desorption process, CC-SA beads were immersed in 100 mL of a NaCl/Ethanol cosolvent mixture (1:3 vol/vol) and agitated continuously at 200 rpm at room temperature for 1 h. Subsequently, the adsorption and desorption were carried out over five cycles to evaluate the adsorbent's recyclability. The experimental results showed that the MB removal capacity was reduced from

Table 5
A comparison of the adsorption capacity for MB on the different materials.

Absorbent	Q_m (mg/g)	References
Chitosan/bentonite beads (CCSB)	95.24	[82]
Chitosan/almond peanut	22.8	[76]
Alg-halloysite hybrid beads	222	[83]
Alginate beads crosslinked	26.6	[84]
Cross-linked chitosan/sepiolite composite	40.986	[85]
Activated oil palm ash zeolite/chitosan (Z-AC/C)	151.51	[86]
Alginate functionalized sugarcane cellulose-based beads (CC-SA)	22.83	This work

85.33 % to 25.83 % in 5 recycling. In general, the first 3 recycling showed that the adsorption efficiency did not change significantly. However, starting from the 4th recycling, the adsorption efficiency started to decrease from about 86 % to 35.8 % and the 5th recycling the efficiency was only 25.83 %. It shows that starting from the 4th recycling, the adsorption activity of the material gradually disappeared, which was caused by the occupancy of the adsorption site by MB [77] or by the oxidation process that vanished or dissolved some of the adsorbent through the treatments [78].

To clarify the interaction of MB and the CC-SA adsorbent, the FT-IR spectra of CC-SA beads with and without MB adsorption were conducted and shown in Fig. 11B. The position changes of the peaks due to MB adsorbed onto CC-SA beads were observed in Fig. 11B. In fact, the peak at 3352 cm^{-1} (-OH, -NH$_2$) shifted to 3182 cm^{-1} and the intensity of this peak was shortened, indicating the formation of a hydrogen bond between the CC-SA adsorbent and MB [79]. The peak at position 1369 cm^{-1} disappeared after the first adsorption indicating an interaction between MB and -COOH and -NH$_2$ groups of the adsorbent [80]. After the first desorption the peaks hardly changed. However, after the 5th treatment, there was a change in the intensity of -OH groups. The peak initially observed at 3182 cm^{-1} shifted to 3318 cm^{-1} with a significant reduction in intensity, suggesting a loss of hydroxyl content or decomposition of the resin. This indicates structural changes in the resin that could affect its adsorption capabilities [79,81]. The above results showed that CC-SA beads are suitable for reusing in 3 times to remove dyes in aqueous solution.

Table 5 displays the MB adsorption capacities achieved by various adsorbents reported in the literature. The adsorbent developed in this study, with its distinctive features such as working in excessive acidic condition, reusability, simple synthesis, and ease of separation, can be utilized as a viable alternative to the commonly used adsorbents for the removal of MB from real-world samples, including industrial wastewater.

4. Conclusions

In this study, CC-SA composite beads were successfully synthesized with self-assembly of cellulose recovered from bagasse and chitosan extracted from shrimp shells with functionalization of sodium alginate. The CC-SA beads had an average diameter of 1.57 ± 0.12 mm, rough surface, many grooves, and pores. The CC-SA beads adsorbed MB with an efficiency of 85.33 % corresponding to a capacity of 4.27 mg g^{-1} at optimal conditions of pH 8, adsorption time 3 h and MB concentration of 10 ppm. The isotherm studies also showed that the adsorption process of MB$^+$ ions on CC-SA adsorbent was a favorable physical adsorption process with multiplayer of MB adsorbed onto its surface. The PSO adsorption kinetic models showed a high correlation with the experimental data while the IPD model showed that it was not the only step determining the MB adsorption rate of CC-SA beads. Especially, the CC-SA beads revealed a potential to industrial application due to its three times of regeneration and being able to work under pH 2.0.

CRediT authorship contribution statement

Huynh Vu Thanh Luong: Writing – review & editing, Writing – original draft, Validation, Methodology, Conceptualization. **Phuoc Pha Le:** Methodology, Data curation. **Quang Quoc Viet Thieu:** Writing – review & editing. **Viet Nhan Hoa Nguyen:** Writing – review & editing. **Thi Nhu Y. Nguyen:** Resources.

Declaration of competing interest

The authors declare that they have no known competing financial interests or personal relationships that could have appeared to influence the work reported in this paper.

Appendix A. Supplementary data

Supplementary data to this article can be found online at https://doi.org/10.1016/j.heliyon.2024.e37860.

References

[1] D.A. Yaseen, M. Scholz, Textile dye wastewater characteristics and constituents of synthetic effluents: a critical review, Int. J. Environ. Sci. Technol. 16 (2019) 1193–1226, https://doi.org/10.1007/s13762-018-2130-z.

[2] N. Tara, S.I. Siddiqui, G. Rathi, S.A. Chaudhry, Inamuddin, A.M. Asiri, Nano-engineered adsorbent for the removal of dyes from water: a review, Curr. Anal. Chem. 16 (1) (2020) 14–40, https://doi.org/10.2174/1573411015666190117124344.

[3] V. Vadivelan, K.V. Kumar, Equilibrium, kinetics, mechanism, and process design for the sorption of methylene blue onto rice husk, J. Colloid Interf. Sci. 286 (2005) 90–100, https://doi.org/10.1016/j.jcis.2005.01.007.

[4] I.A.W. Tan, A.L. Ahmad, B.H. Hameed, Adsorption of basic dye using activated carbon prepared from oil palm shell: batch and fixed bed studies, Desalination 225 (2008) 13–28, https://doi.org/10.1016/j.desal.2007.07.005.

[5] S. Ihaddaden, D. Aberkane, A. Boukerroui, D. Robert, Removal of methylene blue (basic dye) by coagulation-flocculation with biomaterials (bentonite and Opuntia ficus indica), J. Water Process Eng. 49 (2022) 102952, https://doi.org/10.1016/j.jwpe.2022.102952.

[6] R. Begum, J. Najeeb, A. Sattar, K. Naseem, A. Irfan, A. Al-Sehemi, et al., Chemical reduction of methylene blue in the presence of nanocatalysts: a critical review, Rev. Chem. Eng. 36 (6) (2020) 749–770, https://doi.org/10.1515/revce-2018-0047.

[7] T.V.N. Padmesh, K. Vijayaraghavan, G. Sekaran, M. Velan, Biosorption of Acid Blue 15 using fresh water macroalga Azolla filiculoides: batch and column studies, Dyes Pigments 71 (2006) 77–82, https://doi.org/10.1016/j.dyepig.2005.06.003.

[8] K.M. Reza, A. Kurny, F. Gulshan, Parameters affecting the photocatalytic degradation of dyes using TiO_2: a review, Appl. Water Sci. 7 (2017) 1569–1578, https://doi.org/10.1007/s13201-015-0367-y.

[9] C. Galindo, P. Jacques, A. Kalt, Photooxidation of the phenylazonaphthol AO20 on TiO_2: kinetic and mechanistic investigations, Chemosphere 45 (2001) 997–1005, https://doi.org/10.1016/S0045-6535(01)00118-7.

[10] M. Rafatullah, O. Sulaiman, R. Hashim, A. Ahmad, Adsorption of methylene blue on low-cost adsorbents: a review, J. Hazard Mater. 177 (2010) 70–80, https://doi.org/10.1016/j.jhazmat.2009.12.047.

[11] K.B. Tan, M. Vakili, B.A. Horri, P.E. Poh, A.Z. Abdullah, B. Salamatinia, Adsorption of dyes by nanomaterials: recent developments and adsorption mechanisms, Sep. Purif. Technol. 229 (2015) 242, https://doi.org/10.1016/j.seppur.2015.07.009.

[12] W. Mwandira, K. Nakashima, Y. Togo, T. Sato, S. Kawasaki, Cellulose-metallothionein biosorbent for removal of Pb(II) and Zn(II) from polluted water, Chemosphere 246 (2020) 125733, https://doi.org/10.1016/j.chemosphere.2019.125733.

[13] M. Kadhom, N. Albayati, H. Alalwan, M. Al-Furaiji, Removal of dyes by agricultural waste, Sustain. Chem. Pharm. 16 (2020) 100259, https://doi.org/10.1016/j.scp.2020.100259.

[14] A.A. Al-Gheethi, Q.M. Azhar, P.S. Kumar, A.A. Yusuf, A.K. Al-Buriahi, R.M.S.R. Mohamed, et al., Sustainable approaches for removing Rhodamine B dye using agricultural waste adsorbents: a review, Chemosphere 287 (2022) 132080, https://doi.org/10.1016/j.chemosphere.2021.132080.

[15] X. Luo, L. Zhang, High effective adsorption of organic dyes on magnetic cellulose beads entrapping activated carbon, J. Hazard Mater. 171 (2009) 340–347, https://doi.org/10.1016/j.jhazmat.2009.06.009.

[16] A. Mokhtar, S. Abdelkrim, A. Djelad, A. Sardi, B. Boukoussa, M. Sassi, et al., Adsorption behavior of cationic and anionic dyes on magadiite-chitosan composite beads, Carbohydr. Polym. 229 (2020) 115399, https://doi.org/10.1016/j.carbpol.2019.115399.

[17] A. Mokhtari, M. Sabzi, H. Azimi, 3D porous bioadsorbents based on chitosan/alginate/cellulose nanofibers as efficient and recyclable adsorbents of anionic dye, Carbohydr. Polym. 265 (2021) 118075, https://doi.org/10.1016/j.carbpol.2021.118075.

[18] A.A. Oladipo, M. Gazi, E. Yilmaz, Single and binary adsorption of azo and anthraquinone dyes by chitosan-based hydrogel: selectivity factor and Box-Behnken process design, Chem. Eng. Res. Desig. 104 (2015) 264–279, https://doi.org/10.1016/j.cherd.2015.08.018.

[19] A.A. Oladipo, M. Gazi, Enhanced removal of crystal violet by low cost alginate/acid activated bentonite composite beads: optimization and modelling using non-linear regression technique, J. Water Process Eng. 2 (2014) 43–52, https://doi.org/10.1016/j.jwpe.2014.04.007.

[20] S. Hokkanen, A. Bhatnagar, M. Sillanpää, A review on modification methods to cellulose-based adsorbents to improve adsorption capacity, Water Res. 91 (2016) 156–173, https://doi.org/10.1016/j.watres.2016.01.008.

[21] L. Nan, B. Renbi, Copper adsorption on chitosan–cellulose hydrogel beads: behaviors and mechanisms, Sep. Purif. Technol. 42 (3) (2005) 237–247, https://doi.org/10.1016/j.seppur.2008.02.006.

[22] LjS. Čerović, S.K. Milonjić, M.B. Todorovi, M.I. Trtanj, Y.S. Pogozhev, Y. Blagoveschenskii, et al., Point of zero charge of different carbides, Colloids Surf. A Physicochem. Eng. Asp. 297 (2007) 1–6, https://doi.org/10.1016/j.colsurfa.2006.10.012.

[23] I. Langmuir, The adsorption of gases on plane surfaces of glass, mica and platinum, J. Am. Chem. Soc. 40 (1918) 1361–1403, https://doi.org/10.1021/ja02242a004.

[24] H. Freundlich, Über die Adsorption in Lösungen, Z. Phys. Chem. 57 (1907) 385–470, https://doi.org/10.1515/zpch-1907-5723.

[25] C.Y. Abasi, A.A. Abia, J.C. Igwe, Adsorption of iron(III), lead(II) and cadmium(II) ions by unmodified raphia palm (Raphia hookeri) fruit endocarp, Environ. Res. J. 5 (2011) 104–113, https://doi.org/10.3923/erj.2011.104.113.

[26] W.J. Weber, J.C. Morris, Kinetics of adsorption on carbon from solution, J. Sanit. Eng. Div. 89 (2) (1963) 31–60, https://doi.org/10.1061/JSEDAI.0000430.

[27] F.C. Wu, R.L. Tseng, R.S. Juang, Initial behavior of intraparticle diffusion model used in the description of adsorption kinetics, Chem. Eng. J. 153 (2009) 1–8, https://doi.org/10.1016/j.cej.2009.04.042.

[28] P.L. Homagai, K.N. Ghimire, K. Inoue, Adsorption behavior of heavy metals onto chemically modified sugarcane bagasse, Bioresour. Technol. 101 (6) (2010) 2067–2069, https://doi.org/10.1016/j.biortech.2009.11.073.

[29] J. Sun, X. Sun, H. Zhao, R. Sun, Isolation and characterization of cellulose from sugarcane bagasse, Polym. Degrad. Stab. 84 (2) (2004) 331–339, https://doi.org/10.1016/j.polymdegradstab.2004.02.008.

[30] K. Plermjai, K. Boonyarattanakalin, W. Mekprasart, S. Pavasupree, W. Phoohinkong, W. Pecharapa, Extraction and characterization of nanocellulose from sugarcane bagasse by ball-milling-assisted acid hydrolysis, AIP Conf. Proc. 2010 (2010) 020005, https://doi.org/10.1063/1.5053181.

[31] A. Alghooneh, A. Mohammad Amini, F. Behrouzian, S.M.A. Razavi, Characterisation of cellulose from coffee silverskin, Int. J. Food Prop. 20 (11) (2017) 2830–2843, https://doi.org/10.1080/10942912.2016.1253097.

[32] K.O. Reddy, C.U. Maheswari, M.S. Dhlamini, B.M. Mothudi, V.P. Kommula, J. Zhang, et al., Extraction and characterization of cellulose single fibers from native African napier grass, Carbohydr. Polym. 188 (2018) 85–91, https://doi.org/10.1016/j.carbpol.2018.01.110.

[33] A.D. French, Idealized powder diffraction patterns for cellulose polymorphs, Cellul. Chem. Technol. 21 (2014) 885–896, https://doi.org/10.1007/s10570-013-0030-4.

[34] F. Danafar, Recent development and challenges in synthesis of cellulosic nanostructures and their application in developing paper-based energy devices. Cellul, Chem. Technol. 54 (2020) 327–346, https://doi.org/10.35812/CELLULOSECHEMTECHNOL.2020.54.34.

[35] E. Jin, J. Guo, F. Yang, Y. Zhu, J. Song, Y. Jin, et al., On the polymorphic and morphological changes of cellulose nanocrystals (CNC-I) upon mercerization and conversion to CNC-II, Carbohydr. Polym. 143 (2016) 327–335, https://doi.org/10.1016/j.carbpol.2016.01.048.

[36] S. Kumari, R. Kishor, Chapter 1 - chitin and chitosan: origin, properties, and applications, Handbook of Chitin and Chitosan 1 (2020) 1–33, https://doi.org/10.1016/B978-0-12-817970-3.00001-8.

[37] M. Hossain, A. Iqbal, Production and characterization of chitosan from shrimp waste, J. Bangladesh Agric. Univ. 12 (1) (2014) 153–160, https://doi.org/10.22004/ag.econ.209911.

[38] M. Pakizeh, A. Moradi, T. Ghassemi, Chemical extraction and modification of chitin and chitosan from shrimp shells, Eur. Polym. J. 159 (2021) 110709, https://doi.org/10.1016/j.eurpolymj.2021.110709.

[39] M. Mahlous, D. Tahtat, S. Benamer, A.N. Khodja, Gamma irradiation-aided chitin/chitosan extraction from prawn shells, Nucl. Instrum. Methods Phys. Res. B 265 (2007) 414–441, https://doi.org/10.1016/j.nimb.2007.09.015.

[40] H. Aldila, V. Fabiani, D. Dalimunthe, R. Irwanto, The effect of deproteinization temperature and NaOH concentration on deacetylation step in optimizing extraction of chitosan from shrimp shells waste, IOP Conf. Ser. Earth Environ. Sci. 599 (2020) 012003, https://doi.org/10.1088/1755-1315/599/1/012003.

[41] M. Alfatama, L.Y. Lim, T.W. Wong, Chitosan oleate-tripolyphosphate complex-coated calcium alginate bead: physicochemical aspects of concurrent core-coat formation, Carbohydr. Polym. 273 (2021) 118487, https://doi.org/10.1016/j.carbpol.2021.118487.

[42] L. Zhang, C. Huang, C. Zhang, H. Pan, Swelling and dissolution of cellulose in binary systems of three ionic liquids and three co-solvents, Cellulose 28 (2021) 4643–4653, https://doi.org/10.1007/s10570-021-03844-4.

[43] C.-H. Weng, Y.-T. Lin, T.-W. Tzeng, Removal of methylene blue from aqueous solution by adsorption onto pineapple leaf powder, J. Hazard Mater. 170 (1) (2009) 417–424, https://doi.org/10.1016/j.jhazmat.2009.04.080.

[44] J. Yip, C.-W.M. Yuen, C.-W. Kan, H.-C. Cheung, H.-M.P. Leung, K. Cheuk, et al., Chitosan/Clotrimazole microcapsules for Tinea pedis treatment: in-vitro antifungal and cytotoxicity study, J. Text. Inst. 106 (6) (2015) 641–647, https://doi.org/10.1080/00405000.2014.933513.

[45] C. Qin, J. Zhou, Z. Zhang, W. Chen, Q. Hu, Y. Wang, Convenient one-step approach based on stimuli-responsive sol-gel transition properties to directly build chitosan-alginate core-shell beads, Food Hydrocoll 87 (2019) 253–259, https://doi.org/10.1016/j.foodhyd.2018.08.001.

[46] D. Zheng, B. Bai, X. Xu, Y. He, S. Li, N. Hu, et al., Fabrication of detonation nanodiamond@ sodium alginate hydrogel beads and their performance in sunlight-triggered water release, RSC Adv. 9 (48) (2019) 27961–27972, https://doi.org/10.1039/C9RA03914G.

[47] S. Danewalia, K. Singh, Bioactive glasses and glass–ceramics for hyperthermia treatment of cancer: state-of-art, challenges and future perspectives, Mater. Today Bio 10 (2021) 100100, https://doi.org/10.1016/j.mtbio.2021.100100.

[48] K.S.W. Sing, Reporting physisorption data for gas/solid systems with special reference to the determination of surface area and porosity (Recommendations 1984), Pure Appl. Chem. 57 (1985) 603–619, https://doi.org/10.1351/pac198557040603.

[49] P. Jia, H. Tan, K. Liu, W. Gao, Removal of methylene blue from aqueous solution by bone char, Appl. Sci. 8 (2018) 1903, https://doi.org/10.3390/app8101903.

[50] Y. Haiping, C. Rong, L. Hanping, Z. Dong Ho, Z. Chuguang, Characteristics of hemicellulose, cellulose and lignin pyrolysis, Fuel 86 (12) (2007) 1781–1788, https://doi.org/10.1016/j.fuel.2006.12.013.

[51] P. Pereira, H. Voorwald, M.O. Cioffi, D. Mulinari, S. Luz, M. Silva, Sugarcane bagasse pulping and bleaching: thermal and chemical characterization, Bioresources 6 (2011) 2471–2482, https://doi.org/10.15376/BIORES.6.3.2471-2482.

[52] C.G. Flores-Hernández, M.L.A. Cornejo-Villegas, A. Moreno-Martell, A. Del Real, 20201. Synthesis of a Biodegradable Polymer of Poly (Sodium Alginate/Ethyl Acrylate). Polymers 13(4), 504. https://doi.org/10.3390/polym13040504.

[53] W.A. Monal, J.S. Roman, A kinetic study of the thermal degradation of chitosan and a mercaptan derivative of chitosan, Polym. Degrad. Stab. 39 (1993) 21–28, https://doi.org/10.1016/0141-3910(93)90120-8.

[54] J. Soares, J. Santos, G. Chierice, É. Cavalheiro, Thermal behavior of alginic acid and its sodium salt, Eclét. Quím. 29 (2004) 57–63, https://doi.org/10.1590/S0100-46702004000200009.

[55] P. Trivedi, T. Saloranta-Simell, U. Maver, L. Gradišnik, N. Prabhakar, J.-H. Smått, et al., Chitosan–cellulose multifunctional hydrogel beads: design, characterization and evaluation of cytocompatibility with breast adenocarcinoma and osteoblast cells, Bioengineering 5 (1) (2018) 3, https://doi.org/10.3390/bioengineering5010003.

[56] I.M. Fareez, S.M. Lim, R.K. Mishra, K. Ramasamy, Chitosan coated alginate–xanthan gum bead enhanced pH and thermotolerance of Lactobacillus plantarum LAB_{12}, Int. J. Biol. Macromol. 72 (2015) 1419–1428, https://doi.org/10.1016/j.ijbiomac.2014.10.054.

[57] Z. Wang, X. Zhang, J. Gu, H. Yang, J. Nie, G. Ma, Electrodeposition of alginate/chitosan layer-by-layer composite coatings on titanium substrates, Carbohydr. Polym. 103 (2014) 38–45, https://doi.org/10.1016/j.carbpol.2013.12.007.

[58] Y. Jampafuang, A. Tongta, Y. Waiprib, Impact of crystalline structural differences between α-and β-chitosan on their nanoparticle formation via ionic gelation and superoxide radical scavenging activities, Polymers 11 (12) (2019) 2010, https://doi.org/10.3390/polym11122010.

[59] S. Bhagyaraj, I. Krupa, Alginate-mediated synthesis of hetero-shaped silver nanoparticles and their hydrogen peroxide sensing ability, Molecules 25 (3) (2020) 435, https://doi.org/10.3390/molecules25030435.

[60] M.G. Aguayo, A. Fernández-Pérez, C. Oviedo, G. Reyes, P. Reyes-Contreras, Relationship between structural characteristics of cellulose nanocrystals obtained from kraft pulp, Nanomaterials 10 (9) (2020) 1775, https://doi.org/10.3390/nano10091775.

[61] G. Lawrie, I. Keen, B. Drew, A. Chandler-Temple, L. Rintoul, P. Fredericks, et al., Interactions between alginate and chitosan biopolymers characterized using FT-IR and XPS, Biomacromolecules 8 (8) (2007) 2533–2541, https://doi.org/10.1021/bm070014y.

[62] M.G. Sankalia, R.C. Mashru, J.M. Sankalia, V.B. Sutariya, Reversed chitosan-alginate polyelectrolyte complex for stability improvement of alpha-amylase: optimization and physicochemical characterization, Eur. J. Pharm. Biopharm. 65 (2007) 215–232, https://doi.org/10.1016/j.ejpb.2006.07.014.

[63] N.E. Mousa, C.M. Simonescu, R.-E. Pătescu, C. Onose, C. Tardei, D.C. Culiță, et al., Pb²⁺ removal from aqueous synthetic solutions by calcium alginate and chitosan coated calcium alginate, Reac. Funct. Polym. 109 (2016) 137–150, https://doi.org/10.1016/j.reactfunctpolym.2016.11.001.

[64] C. Jiang, Z. Wang, X. Zhang, X. Zhu, J. Nie, G. Ma, Crosslinked polyelectrolyte complex fiber membrane based on chitosan–sodium alginate by freeze-drying, RSC Adv. 4 (2014) 41551–41560, https://doi.org/10.1039/C4RA04208E.

[65] H. Shi, W. Li, L. Zhong, C. Xu, Methylene blue adsorption from aqueous solution by magnetic cellulose/graphene oxide composite: equilibrium, kinetics, and thermodynamics, Ind. Eng. Chem. Res. 53 (2014) 1108–1118, https://doi.org/10.1021/ie4027154.

[66] M. Nishil, G. Nathan, W.H. Ambrose, M.B. Richard, T.K. Chiu, Continuous flow adsorption of methylene blue by cellulose nanocrystal-alginate hydrogel beads in fixed bed columns, Carbohydr. Polym. 136 (2016) 1194–1202, https://doi.org/10.1016/j.carbpol.2015.09.099.

[67] W. Suna, X. Xu, Z. Lv, H. Mao, J. Wu, Environmental impact assessment of wastewater discharge with multipollutants from iron and steel industry, J. Environ. Manage. 245 (2019) 210–215, https://doi.org/10.1016/j.jenvman.2019.05.081.

[68] B.C. Melo, F.A.A. Paulino, V.A. Cardoso, A.G.B. Pereira, A.R. Fajardo, F.H.A. Rodrigues, Cellulose nanowhiskers improve the methylene blue adsorption capacity of chitosan-g-poly (acrylic acid) hydrogel, Carbohydr. Polym. 181 (2018) 358–367, https://doi.org/10.1016/j.carbpol.2017.10.079.

[69] A. Dąbrowski, Adsorption—from theory to practice, Adv. Colloid Interfac. 93 (2001) 135–224, https://doi.org/10.1016/S0001-8686(00)00082-8.

[70] M.G. Vaz, A.G. Pereira, A.R. Fajardo, A.C. Azevedo, F.H. Rodrigues, Methylene blue adsorption on chitosan-g-poly (acrylic acid)/rice husk ash superabsorbent composite: kinetics, equilibrium, and thermodynamics, Water Air Soil Poll 228 (1) (2017) 1–13, https://doi.org/10.1007/s11270-016-3185-4.

[71] P.S. Kumar, P.S.A. Fernando, R.T. Ahmed, R. Srinath, M. Priyadharshini, A.M. Vignesh, et al., Effect of temperature on the adsorption of methylene blue dye onto sulfuric acid–treated orange peel, Chem. Eng. Commun. 201 (2014) 1526–1547, https://doi.org/10.1080/00986445.2013.819352.

[72] A.E. Ofomaja, E.B. Naidoo, A. Pholosi, Intraparticle diffusion of Cr (VI) through biomass and magnetite coated biomass: a comparative kinetic and diffusion study, S. Afr. J. Chem. Eng. 32 (1) (2020) 39–55, https://doi.org/10.1016/j.sajce.2020.01.005.

[73] J.M. Jabar, Y.A. Odusote, K.A. Alabi, I.B. Ahmed, Kinetics and mechanisms of Congo-red dye removal from aqueous solution using activated Moringa oleifera seed coat as adsorbent, Appl. Water Sci. 10 (6) (2020) 136, https://doi.org/10.1007/s13201-020-01221-3.

[74] M. Mohammadi, A.J. Hassani, A.R. Mohamed, G.D. Najafpour, Removal of rhodamine B from aqueous solution using palm shell-based activated carbon: adsorption and kinetic studies, J. Chem. Eng. Data 55 (2010) 5777–5785, https://doi.org/10.1021/je100730a.

[75] J. Sahar, A. Naeem, M. Farooq, S. Zareen, A. urRahman, Thermodynamic studies of adsorption of rhodamine B and Congo red on graphene oxide, Desalin. Water Treat. 164 (2019) 228–239, https://doi.org/10.5004/dwt.2019.24436.

[76] M. Erfani, V. Javanbakht, Methylene Blue removal from aqueous solution by a biocomposite synthesized from sodium alginate and wastes of oil extraction from almond peanut, Inter. J. Bio. Macromol. 114 (2018) 244–255, https://doi.org/10.1016/j.ijbiomac.2018.03.003.

[77] A. Dbik, N. El Messaoudi, S. Bentahar, M. El Khomri, A. Lacherai, N. Faska, Optimization of methylene blue adsorption on agricultural solid waste using box–behnken design (BBD) combined with response surface methodology (RSM) modeling, Biointerface Res. Appl. Chem. 12 (4) (2022) 4567–4583, https://doi.org/10.33263/BRIAC124.45674583.

[78] T.B. Vidovix, H.B. Quesada, R. Bergamasco, M.F. Vieira, A.M.S. Vieira, Adsorption of Safranin-O dye by copper oxide nanoparticles synthesized from Punica granatum leaf extract, Environ. Technol. 43 (20) (2022) 3047–3063, https://doi.org/10.1080/09593330.2021.1914180.

[79] W. Wang, J. Ni, L. Chen, Z. Ai, Y. Zhao, S. Song, Synthesis of carboxymethyl cellulose-chitosan-montmorillonite nanosheets composite hydrogel for dye effluent remediation, Int. J. Biol. Macromol. 165 (2020) 1–10, https://doi.org/10.1016/j.ijbiomac.2020.09.154.

[80] Y. Xia, Q. Yao, W. Zhang, Y. Zhang, M. Zhao, Comparative adsorption of methylene blue by magnetic baker's yeast and EDTAD-modified magnetic baker's yeast: equilibrium and kinetic study, Arab. J. Chem. 150 (2015) 2448–2458, https://doi.org/10.1016/j.arabjc.2015.03.010.

[81] V.-P. Dinh, H.M. Le, V.-D. Nguyen, V.-A. Dao, N.Q. Hung, L.A. Tuyen, et al., Insight into the adsorption mechanisms of methylene blue and chromium (III) from aqueous solution onto pomelo fruit peel, RSC Adv. 9 (44) (2019) 25847–25860, https://doi.org/10.1039/C9RA04296B.

[82] Y. Bulut, H. Karaer, Adsorption of methylene blue from aqueous solution by crosslinked chitosan/bentonite composite, J. Disper. Sci. Technol. 36 (1) (2015) 61–67, https://doi.org/10.1080/01932691.2014.888004.

[83] L. Liu, Y. Wan, Y. Xie, R. Zhai, B. Zhang, J. Liu, The removal of dye from aqueous solution using alginate-halloysite nanotube beads, Chem. Eng. J. 187 (2012) 210–216, https://doi.org/10.1016/j.cej.2012.01.136.

[84] V. Rocher, A. Bee, J.M. Siaugue, V. Cabuil, Dye removal from aqueous solution by magnetic alginate beads crosslinked with epichlorohydrin, J. Hazard Mater. 178 (1–3) (2010) 434–439, https://doi.org/10.1016/j.jhazmat.2010.01.100.

[85] F. Marrakchi, W.A. Khanday, M. Asif, B.H. Hameed, Cross-linked chitosan/sepiolite composite for the adsorption of methylene blue and reactive orange 16, Inter. J. Bio. Macromol. 93 (2016) 1231–1239, https://doi.org/10.1016/j.ijbiomac.2016.09.069.

[86] W.A. Khanday, M. Asif, B.H. Hameed, Cross-linked beads of activated oil palm ash zeolite/chitosan composite as a bio-adsorbent for the removal of methylene blue and acid blue 29 dyes, Inter. J. Bio. Macromol. 95 (2017) 895–902, https://doi.org/10.1016/j.ijbiomac.2016.10.075.